ADVANCED MATERIALS AND ELECTROCHEMICAL FABRICATION METHODS FOR APPLICATION IN BIOSENSORS

By

YINGYING LI, B.ENG.

A Thesis

Submitted to the School of Graduate Studies

In Partial Fulfillment of the Requirements

For the Degree

Master of Applied Science

McMaster University

MASTER OF APPLIED SCIENCE (2010).....McMaster University

(Materials Science & Engineering).....Hamilton, Ontario

TITLE: Advanced materials and electrochemical fabrication methods for application in biosensors

AUTHOR: Yingying Li, B.Eng. (Harbin Institute of Technology)

SUPERVISOR: Professor Igor Zhitomirsky

NUMBER OF PAGES: VII, 123

Abstract

New electrochemical deposition methods have been developed for the fabrication of advanced composite coatings for biosensors applications. The methods are based on electrodeposition of biopolymers, such as cathodic electrodeposition of chitosan, anodic electrodeposition of alginic acid and hyaluronic acid. Another approach is based on electrolytic deposition and electrophoretic deposition of ceramic materials and chitosan. Electrochemical strategies have been discovered for the electrochemical co-deposition of polymers with enzymes, such as glucose oxidase and hemoglobin. Glucose oxidase was used as a model enzyme for the development of new electrochemical strategies for the fabrication of composite coatings for applications in biosensors. New strategies have been further utilized for the fabrication of novel composites containing hemoglobin. It was found that co-deposition of biopolymers and enzymes from the solutions resulted in the fabrication of composite materials which can keep the activity of the enzymes.

Electrochemical methods have been developed for the deposition of composite coatings containing ceramic materials (ZnO) in the matrix of chitosan. The composite coatings can be utilized for the immobilization of enzymes by the electrostatic attraction. The composition and microstructure of the composite coatings were investigated. The composition of these nanocomposite coatings can be varied by variation of bath composition for electrodeposition. The deposition yield was studied at various deposition conditions. Electrochemical deposition mechanisms have been investigated and discussed.

Obtained results pave the way for the fabrication of novel coatings for immobilization of enzymes and for application in advanced biosensors.

Acknowledgement

I would like to express my gratitude to all those who gave me the possibility to complete this thesis.

First of all, I would like to express my sincere appreciation to my supervisor, Professor Igor Zhitomirsky, whose help, stimulating suggestions and encouragement helped me in all the time of research for and writing of this thesis.

Also I would give many thanks to all the team members, Xin Pang, Chao Shi, Rong Ma, for their kindness and friendship.

Last but not the least; I take this opportunity to express my profound gratitude to my beloved parents for their moral support and patience during my study in Canada.

Table of Contents

Table of Figures

1 Introduction

Historically, Dr. Clark first demonstrated the modern concept of biosensors, in which an enzyme was incorporated into an electrode to detect the concentration of glucose. Biological sensors are analytical devices that detect physiological and biochemical changes [1] . Personal blood glucose biosensors are the most successful commercial application of biocatalytic sensors [2].

Enzymes are the oldest and still most commonly used biorecognition elements in biosensors. It has been demonstrated that enzymes are globular proteins composed mainly of the 20 naturally occurring amino acids which can increase the rate of the chemical reactions but without themselves suffering any overall changes. The enzyme-substrate interactions can be characterized by kinetic studies. When preparing a biosensor, many parameters such as origin and availability of the biological component, its operational and storage stability as well as immobilization procedure should be considered [3]. Since biosensor refers to an analytical device, which combines a bioelement and sensorelement, how to immobilize enzyme on the transducer is a problem.

Nowadays, electrodeposition has attracted a lot of attention, because of its advantages such as high purity of deposited materials, to the possibility of uniform

deposition on substrates of complex shape, rigid control of the composition and microstructure of deposits, low cost of equipment and materials, and easy to be scaled up to industry level.

The purpose of this research is to develop an advanced fabrication method for applications of biosensors, including the development of electrodeposition of biopolymers (chitosan, alginic acid, hyaluronic acid) and enzymes (glucose oxidase, hemoglobin) as well as the development of electrodeposition of ceramic materials (ZnO) and biopolymers in order to immobilize enzymes. The electrochemical testing of the modified electrode including enzymes (glucose oxidase) will be discussed in this research.

2 Literature review

2.1 Biosensors and basic concepts

The biosensors' history started from the year of 1962, when enzyme electrodes were developed by the scientist Leland C.Clark. Since then, research groups from different fields such as Chemistry, Physics and Material Science combined their efforts to develop more reliable, stable and sophisticated biosensing devices for applications in the different fields such as agriculture, biotechnology, medicine, military as well as bioterrorism detection and prevention [4].

Depending on the field of applications, the terminologies and definitions of biosensors are different. The names are known as immunosensors, resonant mirrors, chemical canaries, glucose biosensors, biocomputers, etc. A commonly cited definition is described as: a biosensor is a chemical sensing device in which a biologically derived recognition entity is coupled to a transducer in order to allow the quantitative development of complex biochemical parameter [4].

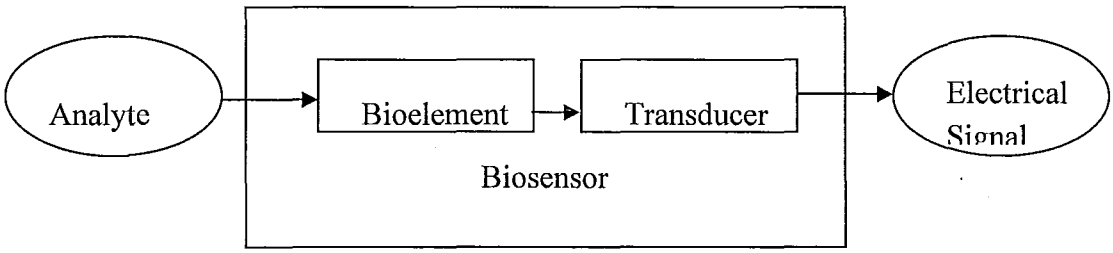

Figure 2-1 Schematic Representation of Biosensors

In **Figure 2-1**, it is demonstrated that a biosensor consists of a bio-element and a sensor-element. Enzyme, antibody, tissue, polysaccharide can act as bioelements, while the sensing element may be electric potential, electric current, electric conductance, mass, temperature, viscosity, etc. There are many applications which are based on various combinations of bio-elements and sensor-elements [4].

Four possible methods which can be used to combine bio-elements and sensor-element are demonstrated in **Figure 2-2**.

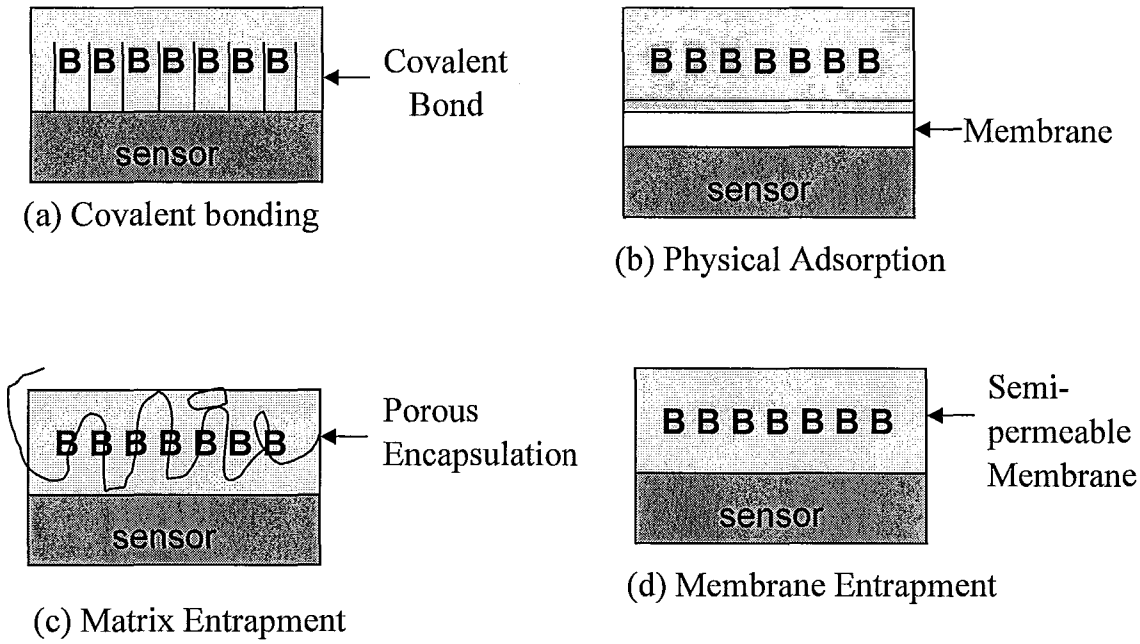

Figure 2-2 Methods for combining bio-elements and sensor-elements

For the covalent bonding **Figure 2-2** (a), the sensor surface acts as a reactive group in order to bind the biological materials. In **Figure 2-2** (b), to attach the biomaterial to the surface of the sensor, the physical adsorption scheme is based on a combination of ionic forces, hydrophobic forces, hydrogen bonds and van der Waals forces. **Figure 2-2** (c) shows the scheme of porous entrapment, which is dependent on forming a porous encapsulation matrix around the biological material thus helping in binding it to the surface of sensors. In the case of membrane entrapment scheme, as **Figure 2-2** (d) shows, analyte and the bioelement are separated by a semi permeable membrane, meanwhile the sensor is attached to the bioelement [4].

2.1 Types of biosensors

2.1.1 Optical-detection biosensors

In optical-detection biosensor, the output transduced signal is measured by using light. This type of biosensor can be based on electrochemiluminescence or optical diffraction. Refer to optical diffraction based biosensors, a silicon wafer is coated with a protein, which forms covalent bonds. This silicon wafer is exposed to UV light through the antibodies from photo mask, then it becomes inactive in the exposed regions. In order to create a diffraction grating, antigen-antibodies bindings are formed in the active regions when the diced wafer chips are incubated in an analyte. When illuminated by a light source such as laser or UV light, a diffraction signal is produced [5].

2.1.2 Resonant biosensors

In resonant biosensors, an acoustic wave transducer is coupled with the bioelement. The output signal is the resonant frequency which can be changed by the change of mass. Thus the mass of membrane will change if the analyte molecule is attached to the membrane [5].

Among the resonant biosensors, the use of surface plasmon resonance biosensors is most popular in various fundamental biological studies such as clinical diagnosis, drug

discovery, health science research, environmental as well as agricultural monitoring. The biosensors of this type have many advantages, for example, the surface plasma biosensors do not require a labeling procedure to measure biomolecular interactions not only qualitatively but also quantitatively.

2.1.3 Thermal-detection biosensors

Unlike the other types of biosensors, thermal-detection biosensors do not need frequent recalibration. They do not require special optical and electrochemical properties of the functional materials. Popular applications of these biosensor include the detection of pathogenic bacteria and pesticides [4]. Thermal-detection biosensors are based on the production or absorption of heat. When the reaction takes place, the temperature of the medium will change. Thermal-detection biosensors usually include enzyme molecules. Once the analyte contacts with the enzyme, the heat reaction of the enzyme is measured and is calibrated against the analyte concentration. This produced total heat is also proportional to the molar enthalpy and the number of molecules in the reaction. So called enzyme thermistors are used for accomplishing the measurement of the temperature [4]

2.1.4 Ion-sensitive biosensors

So called ion-sensitive biosensors are based on the use of semiconductor field effect transistors (FETs) comprising a substrate, an ion sensitive gate, an ion sensitive film, an immobilized enzyme membrane and a Pt electrode. The signal is measured by the changes in the potential when ions and semiconductor interact. The Ion Sensitive Field Effect Transistors (ISFET) are usually constructed by covering the Pt electrode with a polymer layer. This polymer layer must be permeable to the analyte ions. The potential of the FET surface changes when the ions diffuse through the polymer layer [4]. The Pt electrodes of Ion-sensitive biosensors usually have good capabilities of sensing all biological substances which can produce hydrogen peroxide (H_2O_2) in enzyme reaction. They have the rapid reaction time as well as high sensitivity.

2.1.5 Electrochemical biosensors

There are many different types of electrochemical biosensors, including glucose biosensors, immunosensors, and DNA detection biosensors. Such devices provide a simple, inexpensive, accurate and high sensitive platform for patient diagnosis. In this type of biosensor, the electrode transducer is coupled by a biological recognition element thus the biological recognition event can be converted into a useful electrical signal [6].

Electrochemical biosensors can be classified into three types, conductimetric, amperometric and potentiometric.

Conductimetric biosensors detect the changes in the electrical conductance or resistance of the solution, resulting from the electrochemical reactions, which produce ions or electrons. In order to avoid the undesirable effects such as double layer charging, concentration polarization and Faradaic processes, the electric field is generated using a sinusoidal voltage (AC) [4].

In potentiometric biosensors, the analytical information is obtained by converting the biorecognition process into a potential signal using ionselective electrodes [6]. The working principle is based on the fact that when a ramp voltage is applied to an electrode in solution, a current flow is produced due to the electrochemical reactions. So a particular reaction and particular species can be indicated by the voltage at which reactions occur [4].

In amperometric biosensors, the measured parameter is current. Amperometric devices are more attractive due to their wide linear range and high sensitivity. Such biosensors are operated by applying a constant potential and monitoring the current associated with the oxidation or reduction of an electroactive species during the

recognition process [6]. Enzymes are needed to catalyze the production of radio-active species because the biological test samples may not be intrinsically electro-active [4].

2.2 Fabrication methods

2.2.1 Enzyme immobilization

Enzymes are protein molecules acting as biological catalysts which can increase the rate of chemical reactions taking place within living cells without themselves suffering any overall change. Each enzyme is used with a particular substrate to produce a particular product as schematically shown in Figure 2-3.

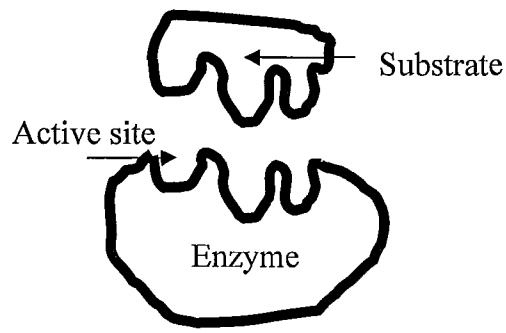

Figure 2-3 A particular enzyme

Nowadays, more and more applications are based on enzyme techniques, because enzymes of high specificity can be selected to desired function. Moreover, little or no by-product formation is observed in the catalytic processes, which can be optimized in very

mild and environmentally-friendly conditions. However, the cost of enzyme preparation is often high, enzymes are intrinsically unstable and easily inhibited. All these problems still need to be solved.

An immobilized enzyme is one whose movement has been restricted either completely or to a small limited region in space such as incorporation in gels, attachment to solid structure, etc. There are plenty of benefits of immobilizing enzymes to a solid support. In this case the enzymes are usually stabilized by chemical binding or electrostatic attraction. This approach offers many advantages. The rapid reaction can be stopped by removing the enzyme from the reaction solution, the product is pure without contamination of enzymes. It also provides possibilities to develop a multienzyme reaction system. Carrier binding, cross linking, entrapment are three common methods for enzyme immobilization. The carrier binding method, which is the oldest immobilization technique for enzymes can be further sub-classified into physical adsorption, ionic binding and covalent binding. In this method the amount of enzymes bound to the carriers and the activities after immobilization are dependent on the properties of the carriers. Cross-linking method is based on the formation of covalent bonds between enzyme molecules, and the formation of three-dimensional crosslinked aggregates. This method is used mostly as a means of stabilizing adsorbed enzymes and

also for preventing leakage, best used in conjunction with one of the other methods. However, cross-linking method may cause loss of enzyme activity during preparation, it may also cause significant changes in the active site of enzymes, and significant loss of activity by severe diffusion limitation. The third method, entrapping enzyme method is based on the localization of an enzyme within the lattice of a polymer matrix or membrane. It can be classified into lattice and micro capsule types. In this method the enzyme is confined in a semi-permeable membrane which allows free passage of low molecular weight molecules but retains the high molecular weight enzyme as shown in **Figure 2-4**.

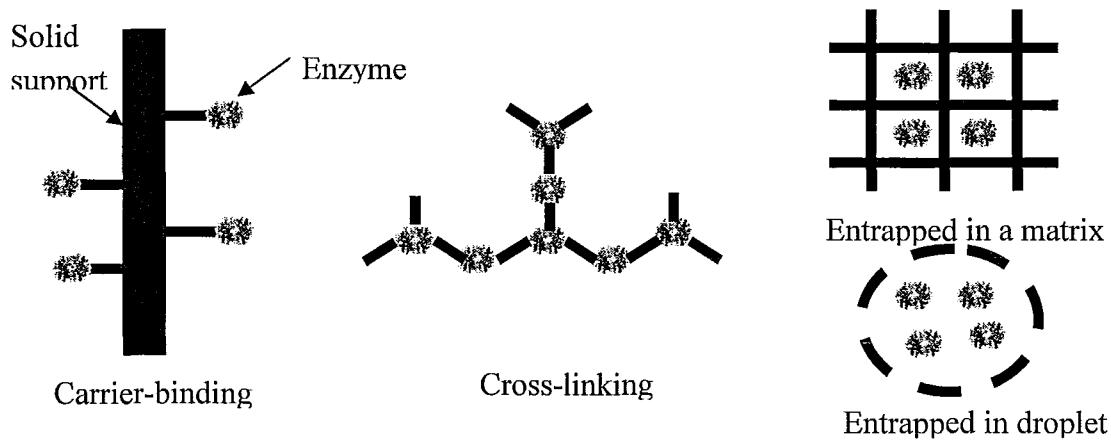

Figure 2-4 Methods for enzyme immobilization

Enzyme immobilization is a common method for applications in glucose biosensors, DNA biosensors and immunosensors. In this method, enzyme electrodes,

which are electrochemical probes with a thin layer of immobilized enzyme on the surface, are often used as working electrodes. Since enzyme can provide the selectivity for the sensor and catalyze the formation of the electroactive product for detection, it is the most important component of the electrodes [7]. The produced current is measured in response to an applied constant voltage, when amperometry monitors the electroactive product directly. The electrode design and solution parameters can determine the activities of the immobilized enzymes, meanwhile, the rate of enzymatic catalysis can also affect the signal in biosensors [7]. The use of enzyme electrodes in biosensors provides many advantages such as simple construction, easily regeneration, reusable and rapid analysis. However, the enzyme layer in the biosensor has to be replaced periodically because it will lose activity gradually [7].

Biosensors based on enzyme electrodes have attracted considerable attention and various chemical and physical schemes have been used to immobilize enzymes on the electrochemical transducers in order to have an intimate contact between the enzyme and the transducer's sensing surface without altering the enzyme geometry or blocking the active parts of the enzyme. The prepared biosensors should be reusable, stable, and maintain the selectivity of the enzyme [8]. However, the number of potential analytes is still larger than the number of available enzyme-based biosensors. A reason for this

phenomenon is due to some disadvantages of enzyme electrode, for example, the enzyme layer in the biosensor has to be replaced periodically since it gradually loses activity, also the chemical detection strategies may be interfered by other redox active species at certain detection potentials. Some factors that prevent wider adaptation of enzyme electrodes still remain, although many successful enzyme electrodes have been fabricated and some sensors have reached the commercial stage. It is still need to discover better ways to overcome the dependence of enzyme activity on the solution conditions such as temperature, pH value, buffer composition, and ionic strength [8, 9]. The solution conditions should remain constant between samples and during the measurements ideally, at the same time, the enzyme should have a wide linear range. According to K.R. Greenough [9], at high concentrations, enzymes become saturated with their substrate due to their active sites becoming the limiting reagent, thus leading to the response signal no longer proportional to the analyte concentration. Based on the expected sensor applications, the amount of enzyme incorporated into the sensor can be adjusted [8].

2.2.2 Glucose biosensors

Diabetes mellitus, which can cause heart disease, kidney failure and blindness, is one of the principal causes of disability and even death in the world. About 200 million people around the world are afflicted with diabetes mellitus, and this figure is expected to

rise up to more than 300 million by the year of 2030 [10, 11]. It is very crucial to test the physiological blood glucose levels in order to avoid diabetic emergencies. Therefore, the development of low cost, high sensitive as well as reliable glucose biosensors has been a concern for several years, not only in medical science research but also in the food industries [10-12].

Glucose oxidase (GOx) has attracted significant attention in the fabrication of glucose biosensors over the last four decades, this is because it can provide sensitivity and reliability for blood glucose monitoring in clinical and biological aspects. However, there are still some disadvantages of enzyme-based glucose biosensors, for example, enzymes immobilization is complicated, operating conditions (optimum temperature, pH value, chemical instability, etc) is critical [10]. The history of glucose enzyme biosensor commenced in 1962 when Clark discovered the first device with oxygen electrode. The first glucose enzyme electrode is called Clark electrode which is based on a thin layer of glucose oxidase entrapped over an oxygen electrode via a semipermeable dialysis membrane. Measurements relied on the monitoring of the oxygen consumed by the enzyme-catalyzed reaction as shown in equation (1).

$$\text{glucose} + O_2 \xrightarrow{\text{glucose oxidase}} \text{gluconic acid} + H_2O_2 \qquad \textbf{(2.1)}$$

A negative potential is applied to the platinum cathode for the reductive detection of the oxygen consumption

$$O_2 + 4H^+ + 4e^- \longrightarrow 2H_2O \qquad (2.2)$$

Clark`s original patent for biosensor covers the use of one or more enzymes for converting electroinactive substrates to electroactive products [13]. The advantage of Clark`s technology is that the effect of interference was corrected by using two electrodes, one of which was covered with the enzyme and measuring the differential current. Subsequently, this technology was transferred to Yellow Spring Instrument (YSI) Company, which launched in 1975 the first dedicated glucose analyzer (the Model 23 YSI analyzer) for direct measurement of glucose in 25 μL whole blood samples [13].

Then, enzyme electrodes are routinely used and are produced commercially in biomedical applications such as glucose testing in clinical laboratories and personal monitoring by diabetic patients. The second - or third- generation biosensors are sold commercially as glucose strips which no longer rely on oxygen as the oxidizing agent, while ferricyanide is still a commonly used mediator for the second-generation sensors. These biosensors typically test a range of 1.1~33.3 mM glucose concentrations with a precision of + 3~8% and test time of about 30 seconds or less [8].

Biocatalytic sensors and some invasive and minimally invasive implantable

glucose biosensors which have an intimate contact between the biocatalytic sensor and the biological tissues or fluids, have been developed. When testing, the minimally invasive blood glucose biosensors are inserted into the arm of a patient. More invasive, intravascular sensors measuring glucose levels in hospitalized diabetes patients are also being developed , however, some problems such as skin irritation, pain, limited lifetime of the sensor and accuracy of the data continue to slow down their wider use [8].

2.2.3 DNA biosensors

During the past few years, it has been demonstrated by the large number of scientific publications in various areas that development of DNA microarrays and DNA biosensors has increased tremendously. In recent years, DNA detection is motivated by applications in a large number of fields, for example, gene analysis, DNA diagnostics, forensic applications and fast detection of biological warfare agents. The detection of genetic mutations at the molecular level provides the possibility of performing reliable diagnostics even before any symptom of a disease appears [14]. Homogeneous assays can be based on electrochemical or optical detection, which allows the determination of DNA sequences. However, they do not allow easily continuous monitoring and miniaturization by these methods while DNA microarrays and DNA biosensors can offer promising alternatives thus allowing continuous, fast, reused, sensitive and selective detection of

DNA hybridization. DNA biosensors or genosensors and DNA microarrays (or called biochips, gene chips, DNA chips) exploit the preferential binding of complementary single-stranded nucleic acid sequences. This system is usually based on the immobilization of a single-stranded DNA probe onto a surface to recognize its complementary DNA target sequence by hybridization. However, transduction of hybridization of DNA could be measured electrochemically, optically, or using mass-sensitive devices [14].

Concerned about the detection mechanism, complementary DNA basepairing is very important, which is the basis for the biorecognition process in hybridization biosensors. These short basepair single-stranded DNA segments which can selectively bind with target analyte are immobilized on the electrode surface. These DNA fragments have to be immobilized in a way that retains their reactivity, stability, accessibility to target analyte and optimal orientation. The surface coverage of the substrates by DNA probes in minimizing nonspecific binding is very important for the DNA biosensors [8]. When target DNA binds to the complementary sequence of the capture or probe DNA in the hybridization process, an electrical signal is produced. Also, this electrochemical signal can result from an electroactive indicator that binds preferentially to DNA duplexes instead of single-stranded DNA probes. A capture enzyme label such as alkaline

phosphatase or horseradish peroxidase can also be used as a measure of hybridization. Nanoparticle labels, for example, colloidal gold have been used to quantify binding. In order to achieve high selectivity and sensitivity, the experimental conditions, like other biological macromolecules with complex structures, ionic strength, temperature, and time allowed for hybridization, have to be controlled well [8].

Based on the selective reaction between target DNA and a DNA capture probe immobilized on the electrode surface in the sample, an electrochemical sensor has been commercialized by Osmetech. This DNA biosensor uses a sandwich type assay as shown in **Figure** 2-5.

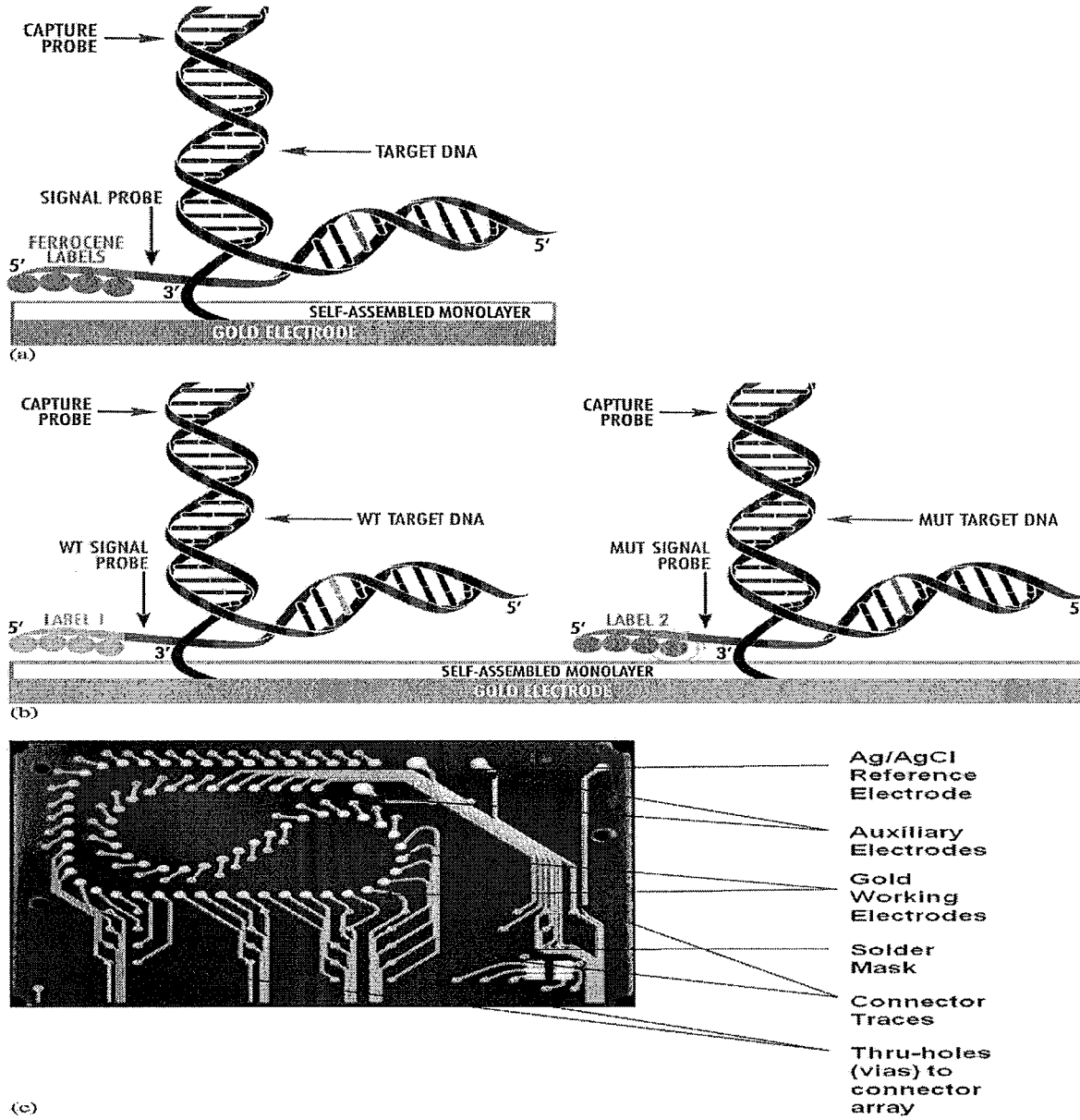

Figure 2-5 Commercially available electrochemical DNA sensor by Osmetech:

(a) detection prin ciple, (b) assay genotyping principle, (c) disposable biosensor printed circuit [8].

Chemical layer attached to the gold electrode is created by self-assembled monolayer technology. Gold immobilizes the DNA using a special alkane thiol linker that projects it beyond a layer of shorter alkane thiols. The capture probe is designed to be shorter than the complementary target strand in order to leave a segment on the target DNA, where a signal probe containing an electroactive label can bind. As shown in **Figure 2-5** (b), different ferrocene labels with distinguishable electrochemical potentials for each label are used for genotyping **Figure 2-5** (c) shows the biochip which consists of a microarray of a Ag/AgCl reference ,72 working electrodes, and two auxiliary electrodes [8].

2.2.4 Immunosensors

The structures of antibodies are very similar. There are five classes of immunoglobulins (IgA, IgD, IgE, IgG and IgM), which only differ in, for example, glycosylation and number and positions of the disulfide bridges. Mainly IgG is used for immunosensors as shown in Figure 2-6. An IgG consists of two heavy and two light chains, which are interconnected by disulfide bridges. All chains have a constant and variable region. The variable regions of the heavy and light chain combine in one interaction site for the antigen, which is called the antigenic site. Therefore, an IgG molecule has two identical binding locations for the antigen [15].

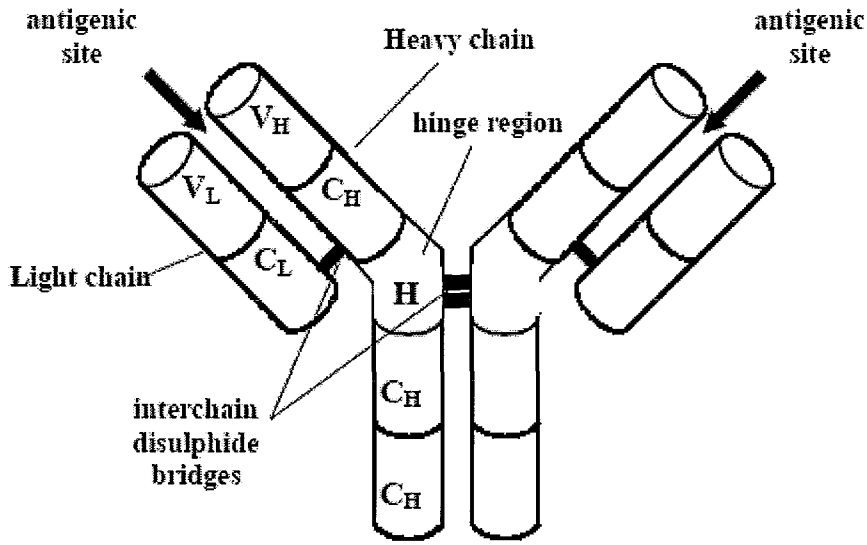

Figure 2-6 The structure of an IgG molecule [15].

Generally, in case of an immunosensor, the sensing element is formed by immobilized antibodies or antigens.

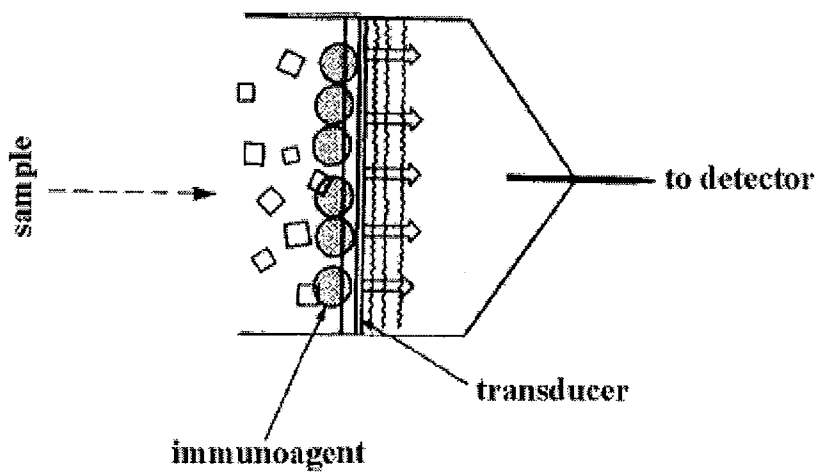

Figure 2-7 Principle of operation of an immunosensor [15].

Like DNA, enzymes, and other biorecognition molecules, antibodies are very sensitive to their environmental conditions. In an immunosensor, typically antibodies have to be immobilized on a solid surface thus leading to loss of their orientation on the solid surface. Amperometric detection systems have been demonstrated to be the most suitable means for immunosensor construction, compared to other electrochemical techniques such as potentiometric and conductimetric, due to their high sensitivity, low cost and the possibility of instrument miniaturisation. A large number of antibody-enzyme or antigen-enzyme conjugates are commercially available since enzyme labels provide great signal amplification in the assay. The majority of amperometric immunosensors (or immunoassays) relies on the use of specific enzyme/substrate couple. The disadvantage of the immunosensors, based on the use of conventional electrodes, is the regeneration of the binding sites of the antibodies bound to the immunosensors surface. This regeneration, using alkaline or acidic solutions, is time-consuming and potentially harmful to the binding capacity, also it may lead to a diminished lifetime of the immobilized antibodies or to serious drift problems [16].

2.3 Polymers for application in sensors

2.3.1 Conducting polymers

In order to entrap enzymes in polymeric enzyme sensors, conducting polymers have been developed, which were first described by Foulds and Lowe in the 1980s. These conducting polymers have a large number of advantages such as high conductivity and stability. The thickness of the polymer film, which is related to the response time of an enzyme electrode, can be controlled by the charge consumed in the polymerization of monomer. These films can be prepared in a one-step process from either aqueous solutions or organic suspensions, also, they are generally homogeneous, chemically stable and adhere strongly to the electrode surface. All of these factors play an important role in the stability of the immobilized enzyme and the response time of an enzyme electrode. The immobilization of an enzyme with a conducting polymer has attracted considerable attention because of the use of a conducting polymer as a support material [17].

2.3.1.1 Polyaniline (PANI)

Polyaniline (PANI) is a conducting polymer of the semi-flexible rod polymer family. Only recently polyaniline captured the attention of the scientific community due

to the discovery of its high electrical conductivity, although it was discovered over 150 years. It has improved stability and conductivity compared to other conducting polymer such as PPY, and polyaniline (PANI). The PANI-GOx electrode obtained by electrochemical immobilization had a fast response and remained stable for a long period of storage [18]. A new biosensor was prepared using a thin layer of PANI incorporating GOx. The operational mechanism was based on the change in electronic conductivity in response to changes in the microenvironment such as pH value or redox potential of the solution in contact with the polymer. The conductivity of a PANI film was controlled by pH changes produced by the production of gluconic acid in a PANI/Gox overlayer [19]. The advantage of the enzyme switches is that the enzyme can supply the required substrate selectivity for the resulting device and that the sensors are fast responsive. In addition, PANI was used in preparation of the biosensor in a nonaqueous phase. It was reported a reagentless amperometric organic phase enzyme electrode employing covalently attached horseradish peroxidase and an electrochemically deposited ferrocence-mediated PANI film on a glassy carbon electrode [17].

2.3.1.2 Polypyrrole (PPY)

Polypyrrole (PPY) is the material of choice for most researchers, usually in combination with glucose oxidase (GOx), which can generate H_2O_2 that is oxidized at

the substrate electrode. The catalytic reactions mainly occur at the PPY - solution interface It is concluded that the rate of electron transfer increased significantly when a small electron-transfer protein, cytochromec, was entrapped within PPY. A role for the PPY was proposed in enhancing electrochemical communication between the electrode and enzymes [17]. In order to improve enzyme activity and stability, several papers addressed the issue of electropolymerization procedures. In some methods, the modified enzyme is subsequently electrochemically polymerized using free pyrrole monomers to produce electrogenerated films containing covalently immobilized enzyme. The stability of the immobilized enzyme as well as the amount of incorporated enzyme and reproducibility of the activity of deposited material was improved [20] .

An improved glucose sensor was fabricated by entrapping the enzyme GOx during polymerization of pyrrole onto a platinum electrode using either amperostatic or potentiostatic electrochemical techniques. The sensor was quite stable for a long time and showed less interference from ascorbic acid with higher GOx concentrations. In other applications involving enzymes entrapped within PPY, it was demonstrated the possibility of controlling the activity of the entrapped enzyme via anion doping or undoping using phosphate and pyruvate oxidase. The catalytic role of the enzyme in the PPY-urease film, which relies on the conversion of urea to carbon dioxide and ammonia,

was used for the detection of urea by the use of both spectrophotometric and potentiometric methods [17].

2.3.2 Biopolymers

2.3.2.1 Chitosan

Chitin is a natural biopolymer originating from the shells of shrimp and other sea crustaceans. It is the second most abundant organic resource on the earth just behind cellulose and is estimated to be synthesized and degraded in the vast amount of billions of tons each year in the biosphere [21].

In chemical definition, chitin consists of β linked 2 -acetamido- 2-deoxy-β- D-glucose units (or N-acetyl-D-glucosamine) [22]. This long chain linear polymer is insoluble in most solvents, which is a major problem for the development of processing techniques and for its applications. This property also is a barrier to determine its molecular weight, which is very important for the determination of properties of the polymers. It also results in a lack of data on the physical properties of chitin in solution. The first well-developed study on chitin solubility was published by Austin [23, 24], who introduced methods of chitin dissolution in numerous solvents. Later, a few papers were published which discussed the preparation of alkali chitin by dissolution of chitin at low

temperature in NaOH solution [25, 26]. They found that in order to get water solubility, the degree of deacetylation of chitin has to be around 50%.

Chitosan is the product of alkaline deacetylation of chitin. However, the deacetylation process is rarely complete, so chitosan showed a partially deacetylated structure in Figure 2-8. Chitosan has a large number of properties which makes it the most important derivative of chitin for biomedical applications. First of all, the amino groups of chitosan have a pKa value around 6.5, which results in the formation of only pseudonatural cationic polymer [27-29]. Secondly, the cationic chitosan can have electrostatic interactions with anionic glycosaminoglycans (GAG) and other negatively charged surfaces such as mucous membranes, therefore, chitosan is a bioadhesive polymer. It also known that the amino group of chitosan are reactive, which can employ many chemistries to functionalize chitosan or cross-link the chitosan backbone to confer elasticity [30].

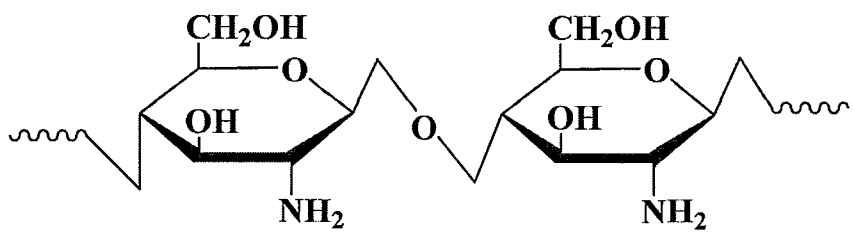

Figure 2-8 The structure of chitosan

Chitosan also has many other specific advantages for biomedical applications such as antimicrobial properties, good biocompatibility, excellent film forming properties. etc. These generate great interest of many researchers and industries for applications of chitosan. Layer-by-layer polyelectrolyte capsules and chitosan gels are often used for controlling release of drugs or proteins [31]. Wound dressing and tissue engineering applications also have been presented [32, 33]. Chitosan coatings containing hydroxyapatite were prepared by electrophoretic deposition for the modification of surface properties of implants [34-36].

2.3.2.2 Alginic acid

Alginic acid, also called alginate or algin, is an anionic polysaccharide distributed widely in the cell walls of brown algae, where it, through binding water, forms a viscous gum. In extracted form it absorbs water quickly; it is capable of absorbing 200-300 times its own weight in water. Its colour ranges from white to yellowish-brown. It is produced in filamentous, granular or powdered forms. The annual production of alginates is around 40,000 tons and 30% is used in food and beverage industry. However, the biomedical application for this natural biopolymer has attracted a lot of attention recently.

Alginic acid is a linear copolymer with homopolymeric blocks of β-D-mannuronate (M) and its C-5 epimer α-L-guluronate (G) residues, respectively, covalently linked together in different sequences or blocks. The monomers can appear in homopolymeric blocks of consecutive G-residues (G-blocks), consecutive M-residues (M-blocks), alternating M and G-residues (MG-blocks), or randomly organized blocks, as shown in Figure 2-9.

At low pH, alginates can form acidic gels by hydrogen bonds. The homopolymeric blocks form the junctions, however, the stability of the gel is mostly dependent on the content and length of G blocks [37]. This gel formation property combined with other advantages like biocompatibility, biodegradability, non-toxicity, low cost and availability, paves an extensive way for biomedical application of alginates. Alginates can also be fabricated as capsules, fibers, beads, and films and then be used as haemostatic materials and wound dressings [38]. In the tissue engineering area, alginates can be used to alter the surface properties of biomedical implants, combining with other biomaterials like hyaluronic acid, chitosan, proteins and drugs [39].

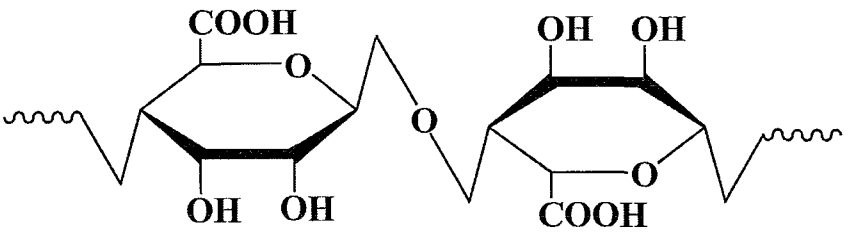

Figure 2-9 The structure of alginic acid

2.3.2.3 Hyaluronic acid

Hyaluronic acid (or called hyaluronan or hyaluronate) was extracted the first time from vitreous humor of cattle eyes by Meyer in 1934 [40]. It exists in all mammals and is identical in all species and tissues, which can be isolated from numerous sources such as rooster combs, bovine vitreous humor, or umbilical cords etc. However, the price of this type of naturally extracted hyaluronic acid is very expensive, also certainly associated with some proteins which can not be removed clearly. Recently, a large production of hyaluronic acid with high purity was achieved using bacteria such as Streptococcus zooepidemicus and Streptococcus equi .

The chemical structure of hyaluronic acid is shown in Figure 2-10. It is a linear polysaccharide composed with alternating N-acetyl-D-glucosamine (GlcNAc) and D-glucuronic acid (GlcA) units. There is a large number of unique properties of hyaluronic acid for biomedical applications. First of all, it has interesting viscoelastic and hydrating

properties resulting from the semiflexible properties of hyaluronic acid chains and the interactions between chains. Secondly, its water binding capacity gives structure to tissues, lubricate joints and muscles. It also has good biocompatibility and autocrosslinking capacility due to the reaction between –OH and –COOH.

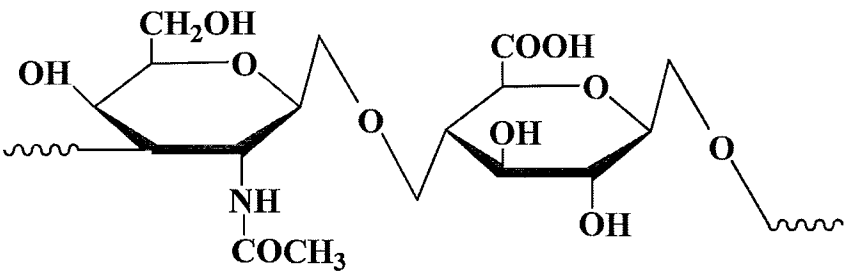

Figure 2-10 The structure of hyaluronic acid

Hyaluronic acid coatings are used for surface modification and tissue reconstruction for bone, cartilage and skin repair based on the prevention property of post-surgical tissue adhesion combined with its biocompatibility [41]. In addition, hyaluronate coatings improved the biocompatibility of the luminal surfaces of small caliber artificial grafts. In vitro studies showed that the platelet adhesion on the coated surfaces was reduced significantly [42].

2.4 Electrodeposition

2.4.1 Introduction to electrodeposition

Generally, electrodeposition is defined as the deposition of a substance on an electrode by the action of electricity, especially by electrolysis. It was discovered by Luigi V. Brugnatelli, who was an Italian professor, by electrodepositing gold on the surface of a metallic object in 1805. Then, electrodeposition really took off with development of effective electrolytes for silver and gold deposition around 1840. These have been the basis of an extraordinarily successful decorative plating industry. However, the electrolytes were very toxic, as they incorporated cyanide, and the search for safer, better substitutes continues [43]. Electrodeposition offers a large number of advantages compared with other surface modification techniques, such as low cost of equipment and materials, easy scale up to industry level, high purity of deposited materials, the possibility of uniform deposition on substrates of complex shape, rigid control of the composition and microstructure of deposits. All these properties contribute to a significant interest in the application of electrochemical processing techniques for the fabrication of thin film, fibers and coatings for biomedical applications [44-46]. There are two prominent techniques in electrodeposition: electrophoretic deposition (EPD) and electrolytic deposition (ELD). EPD is a process in which charged particles, suspended in

a liquid medium, migrate and deposit on an electrode under the influence of an electric field. ELD is a process in which particles are produced in electrochemical reactions from solutions of metal salts and precipitate at the electrode surface to form a deposit. The differences between these two mechanisms are shown in **Figure 2-11**[47]. It is very important to note that the deposit formation in both EPD and ELD processes is achieved via particle coagulation. It is also crucial to understand of the mechanism of particle coagulation.

The classical Derjaguin-Landau-Verwey-Overbeek (DLVO) theory of colloidal stability can be used for the understanding of EPD and ELD deposition mechanisms through particle interaction considerations.

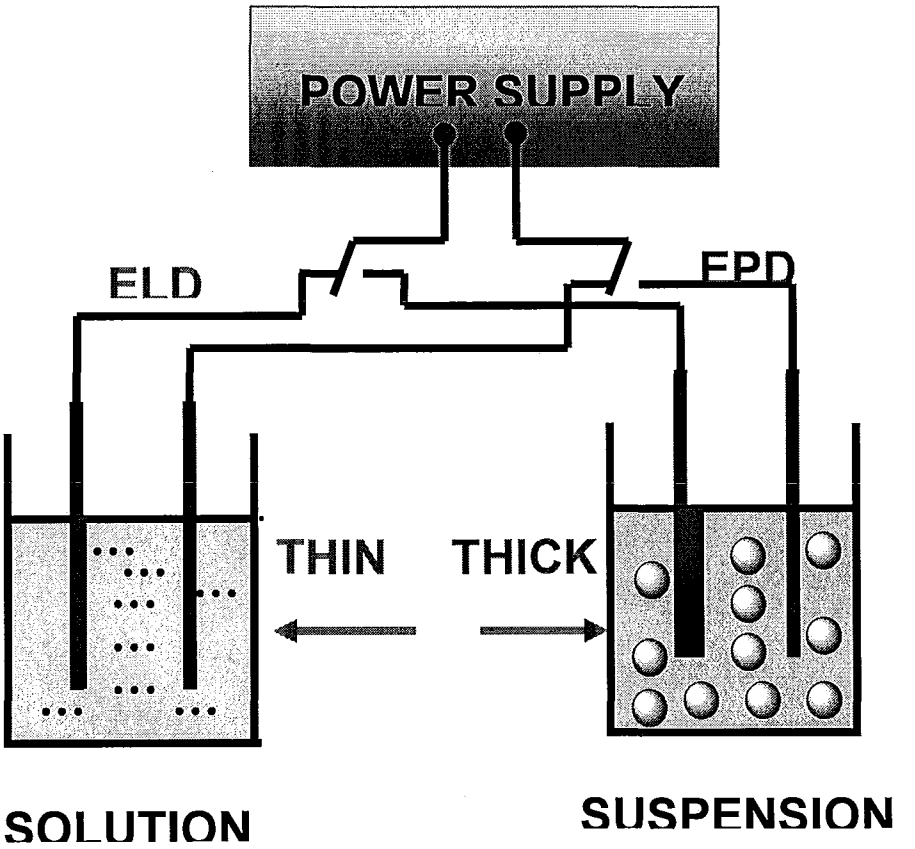

Figure 2-11 Schematic of cathodic electrophoretic deposition (EPD) and electrolytic deposition (ELD)

2.4.1.1 The DLVO theory

The DLVO theory described the relationship between stability of suspensions and energies of interactions between colloidal particles and other surfaces in a liquid quantitatively [48, 49]. According to this theory, the stability of a colloidal system is determined by the total pair interaction between colloidal particles, which is composed of coulombic double-layer repulsion and Van der Waals' attraction.

The total energy V_T of interaction of two isolated, identically charged particles can be defined as:

$$V_T = V_A + V_R \qquad \textbf{(2.3)}$$

The attractive energy V_A is the London-van der Waals' interaction between two spherical particles can be expressed by:

$$V_A = -\frac{A}{6}\left(\frac{2}{s^2-4} + \frac{2}{s^2} + \ln\frac{s^2-4}{s^2}\right) \qquad \textbf{(2.4)}$$

where A is the Hamaker constant and s = 2 + H/a, H is the shortest distance between the two spheres with a the particle radius. If H << a, Equation (2.4) can be simplified to:

$$V_A = -A\frac{a}{12H} \qquad \textbf{(2.5)}$$

The repulsive energy V_R is the coulombic double-layer repulsion which can be expressed by:

$$V_R = 2\pi\varepsilon\varepsilon_0 a\psi^2 \ln[1 + e^{-\kappa H}] \qquad \textbf{(2.6)}$$

where ε is the dielectric constant of the solvent, ε_0 is the dielectric permittivity of free space, ψ is the surface potential, 1/κ is the Debye length:

$$\kappa = \left(\frac{e^2 \sum n_i z_i^2}{\varepsilon\varepsilon_0 kT}\right)^{1/2} \qquad \textbf{(2.7)}$$

where e is the electron charge, k is the Boltzmann constant, T is the absolute temperature, n_i is the concentration of ions and valence z_i. Repulsion between colloidal particles is directly related to the diffuse layer charge on the particles.

The DLVO theory describes the potential energy curve for pair interaction, as shown in **Figure 2-12** (a). When the diffuse-layer repulsion is sufficiently high compared to the van der Waals' attraction, the total energy of particle interaction exhibits a maximum, which makes an energy barrier to particle coagulation.

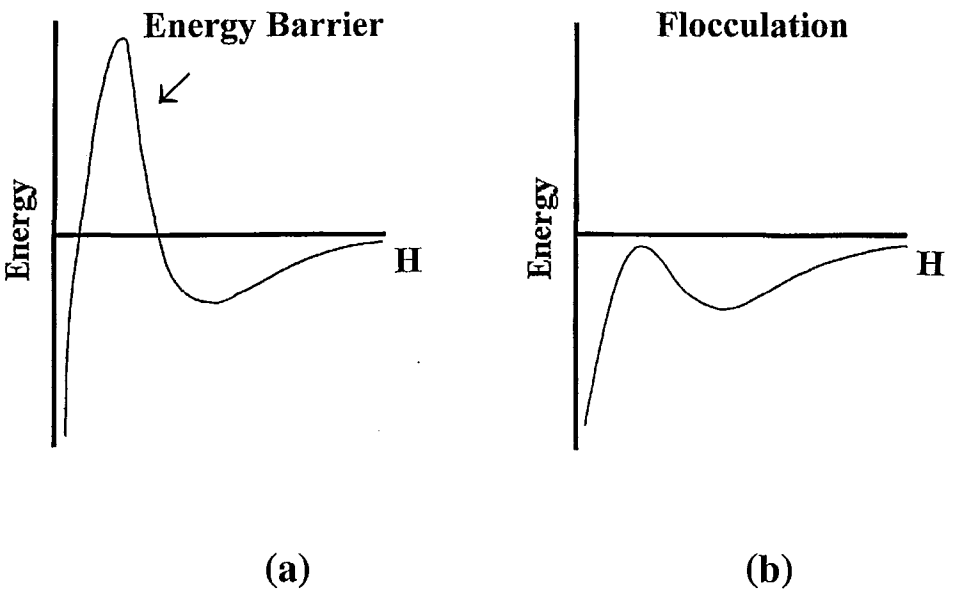

Figure 2-12 Total interaction energy between spherical particles as a function of interparticle separation according to the DLVO theory.

The thickness of the double layer (characterized by the Debye length, $1/\kappa$) is very sensitive to the electrolyte concentration. The DLVO theory explains the existence of a critical electrolyte concentration (flocculation value) for coagulation, decreasing with the

valence of the electrolyte ions of a charge opposite to that of the colloidal particles (rule of Schulze and Hardey [48, 49]). It was demonstrated that the potential energy peak decreases as the electrolyte concentration increases. It is shown in **Figure 2-12** (b), as the energy barrier disappears, coagulation becomes possible. However, the flocculation values are affected by many factors such as sol concentration, temperature, particle size of the colloid, and chemical nature of the sol.

2.4.1.2 Solvent

The solvent is a very important factor for electrodeposition, since it acts as a vehicle that carries the particles in suspensions (EPD) or ions in solution (ELD). For EPD, solvents should be inert with respect to the powder. Organic solvents are preferable for EPD in order to avoid gas evolution from the electrolysis of water. For cathodic ELD of oxide materials, a sufficient amount of water is needed for base generation. However, adsorbed water in green deposits leads to film shrinkage and cracking during drying. The addition of alcohol to aqueous solutions reduces the total dielectric constant of the solvent thus reducing the solubility of the deposits.

2.4.1.3 Suspension stability and particle charging

The charged particles in suspension electrophoretically move in response to the electric field. The so called double-layer is a layer around, a charged particle in a suspension, which consists of ions with an opposite charge in a concentration higher than the bulk concentration of these ions [50]. When an electric field is applied, a fraction of the ions surrounding the particle will not move in the opposite direction but move along with the particle. The potential at this surface of shear is defined as the ζ potential or electrokinetic potential. Surfaces of oxide particles dispersed in water tend to coordinate water molecules to form hydroxylated surfaces. The surfaces may become positively or negatively charged, depending on pH:

$$M\text{-}OH + H^+ \Leftrightarrow M\text{-}OH_2^+ \quad \textbf{(2.1)}$$

$$M\text{-}OH + OH^- \Leftrightarrow M\text{-}O^- + H_2O \quad \textbf{(2.2)}$$

According to the DLVO theory, colloidal stability is closely related to the ζ potential of the colloidal particles. For aqueous suspensions of ceramic powders, especially oxides, the ζ potential changes with pH if H^+ and OH^- are potential-determining ions, showing an isoelectric point (IEP) **Figure 2-13.** ζ potential is positive at low pH values and negative for high pH values.

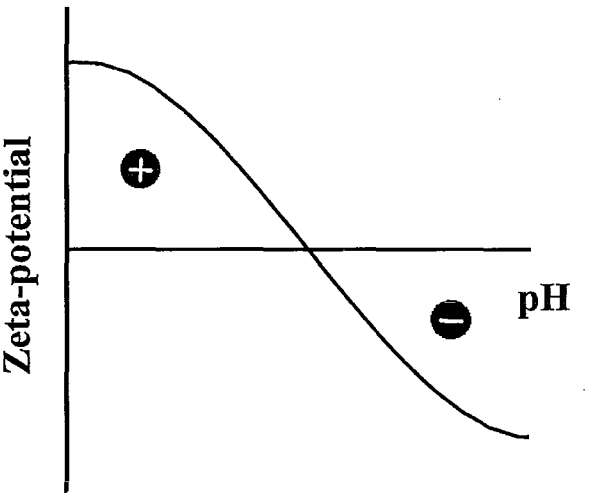

Figure 2-13 ζ potential of ceramic particles versus pH of suspension.

2.4.2 Mechanism of EPD

Electrophoretic deposition (EPD) is achieved via the motion of charged particles towards an electrode under the influence of an electric field and deposition of the particles at the electrode surface [51]. The mechanisms of EPD have been discussed in various publications. One hypothesis, is that charged particles undergo reactions at the electrode, which reduce their surface charge or neutralize them. A difference in pH near electrodes compared with the rest of the suspension is believed to play a major role in this reduction of charge.

There are two types of EPD processes: anodic and cathodic processes. In aqueous solutions, the electrolysis of water is the major electrochemical process which can be shown by the following two electrode reactions:

$$\text{Anode: } 2H_2O \rightarrow O_2 + 4H^+ + 4e^- \qquad \textbf{(2.10)}$$

$$\text{Cathode: } 4H_2O + 4e^- \rightarrow 4OH^- + 2H_2 \qquad \textbf{(2.11)}$$

In anodic EPD, the negatively charged particles react with the positively charged hydrogen ions (protons) which are produced by the reaction (**2.10**) at the anode. Then the neutralized particles form deposits at the anode. In cathodic EPD the positively charged colloidal particles are neutralized by electrogenerated base produced in reaction (**2.11**) and form cathodic deposits. According to Hamaker and Verwey [52, 53], the deposition yield in the electrophoretic process can be described by the Hamaker equation:

$$Y = \mu EtSC_s \qquad \textbf{(2.12)}$$

where Y is the mass of a deposit obtained during deposition time t on the electrode area S, and μ and C are mobility and concentration of polymer macromolecules or inorganic particles, respectively.

This equation gives us a useful starting point for the refinement of the description of deposit formation rates in the EPD process. However, it only describes the EPD process from suspensions containing single component particles. Further work is still

needed for the development of theories of electrophoretic co-deposition process. Recently, Zhitomirsky and Granfield [54] demonstrated that EPD enables the co-deposition of hydroxyapatite (HA) and silica to form HA-silica-chitosan coatings on various conductive substrates. This novel nanocomposite material can also be used for surface modification of metal implants.

2.4.3 EPD of organic-inorganic composite coatings

Organic-inorganic composite materials have generated substantial attention because they can combine the properties of both organic and inorganic components [55-57]. Self-assembly method is usually used for the fabrication of organic-inorganic nanocomposites containing polyelectrolytes and inorganic nanoparticles [58, 59]. However, many authors used polyelectrolyte multilayers and polyelectrolyte capsules as reactors for the synthesis of inorganic nanoparticles [60, 61]. EPD is another promising method for fabricating composite films containing polyelectrolytes and inorganic nanoparticles. EPD has a large number of advantages such as short processing time and process simplicity. In addition, uniform films of controlled composition can be obtained on the substrates of complex shape as well as on selected areas of the substrates [62].

Polyelectrolytes, which are macromolecules that contain charged functional groups, have important role in EPD. Polyelectrolytes can be classified into two groups,

strong polyelectrolytes with the degree of ionization is independent of the solution pH, and weak polyelectrolytes, for which the degree of ionization is determined by the solution pH value. Poly (diallyldimethylammonium chloride) (PDDA), because of the quaternary ammonium group is a strong polycation [45]. Chitosan (CHIT), poly (ethylene imine), Poly (vinylamine) (PVA) are weak polyelectrolytes,containg amine groups [62].

Complexes composed of a polymer ligand and metal ions in which the metal ions are attached to the polymer ligand by a coordinate bond are defined as polymer-metal complexes. A polymer chelate is formed when a metal ion is added to a solution of a polymer ligand such as CHIT, PVA. The suspension must be colloidally stable in order to combine EPD of strong polyelectrolytes and electrosynthesis of inorganic nanoparticles. Deposit formation is achieved via the coagulation of the colloidal particles accumulated at the electrode [45]. The charge compensation mechanism for the fabrication of organic-inorganic nanocomposites containing PDDA has been developed [63]. PDDA macromolecules maintain a high positive charge in acidic bulk solutions as well as in basic conditions at the cathode surface. From aqueous PDDA solutions, no deposit formed because of the strong electrostatic repulsion of the PDDA macromolecules, however, co-deposition of PDDA and the colloidal particles of metal oxides or

hydroxides was observed [47, 62, 64, 65]. It was suggested that the deposit formation is driven by Coulombic attraction between two charged species : negatively charged colloidal particles and cationic PDDA formed at the electrode surface [45].

The co-deposition of PDDA and oxides is also very important for the fabrication of thick oxide films by EPD. The PDDA acts as a binder, providing better adhesion of the deposits and preventing cracking. In addition, positive charge of PDDA can compensate the negative charge of the inorganic nanoparticles [62]. Pang and Zhitomirsky have shown the possibility to obtain relatively thick ceramic films using small PDDA additives as a binder [66].

pH can be used as a tool to manipulate the charge and solubility of the polymers for weak polyelectrolytes. CHIT has pH-responsible electrostatic and solubility properties which allow it to be deposited on the cathode surface [67-69]. The protonated CHIT is a soluble cationic polyelectrolyte which can be neutralized by the electrogenerated base to form an insoluble deposit at the cathode surface:

$$CHIT—H^+ + OH^- \rightarrow CHIT + H_2O \qquad \textbf{(2.13)}$$

Depending on the deposition time, applied voltage, and the CHIT concentration in the solution, the thickness of the CHIT films prepared by EPD was varied from tens of

nanometers to micrometers [62, 67]. It was demonstrated that CHIT promotes the EPD of the latex nanoparticles, which were uniformly distributed in the CHIT film [70].

There is an obstacle in assembling and maintaining a nanoscale material, which is the tendency itself to aggregate. To solve this problem, the nanoparticles can be formed by electrosynthesis in situ in a polymer matrix by the combined deposition method based on the use of cationic polyelectrolytes or polymer-metal ion complexes. In the cathodic electrosynthesis, colloidal particles are formed on the electrode due to the high pH of the cathodic region. The pH increase at the cathode surface results in a decreasing charge and promotes the deposition of weak polyelectrolytes [62]. In addition, EPD of polyelectrolytes can also be combined with electrosynthesis of inorganic nanoparticles to form nanocomposite films.

3 Objective

- Fabrication and testing of electrochemical biosensors
  - Development of advanced methods for immobilization of enzymes
  - Development of composite chitosan-zinc oxide nanocomposites by electrophoretic deposition and electrosynthesis for immobilization of enzymes
  - Development of composite coatings containing glucose oxidase, hemoglobin in matrix of biopolymers: chitosan, alginic acid, and hyaluronic acid.
- Investigation of the deposition mechanism, kinetics of the deposition, deposit composition and microstructures.
- Electrochemical testing of the electrochemical biosensors.

4 Experimental Procedures

4.1Materials

4.1.1 Materials purchased from commercial suppliers

The materials listed in the **Table 4-1** were used for the fabrication of coatings by electrodeposition.

Table 4-1 Materials purchased from commercial suppliers

Material	Supplier	Purity and other specifications
Sodium alginate	Aldrich	Mw 12,000-80,000
Sodium hyaluronate	Alfa Aesar	Mw 100,000-200,000
Hemoglobin	Sigma	≥ 96%
Glucose oxidase	Sigma	50KU,~75% protein
Chitosan	Aldrich	Mw 150,000-200,000 (from crab shells) Degree of deacetylation -85%
Zinc acetate	EM Science	FW 219.51
Acetic acid	Caledon Laboratories Ltd	Reagent grade
Ethanol	Commercial Ethanol Inc.	Reagent grade
Zinc oxide	Aldrich	Nanopower, <100nm
PBS	Sigma	0.01M/L Ph=7.4

4.2 Coating fabrication by electrodeposition methods

4.2.1 Experimental setup for electrodeposition

Cathodic and anodic electrodeposition was used for the fabrication of the polymer-enzyme (protein) and ceramic-polymer composite coatings. Figure 4-1

Schematic of the setup of the deposition cell shows the schematic of the setup of the electrochemical cell for deposition.

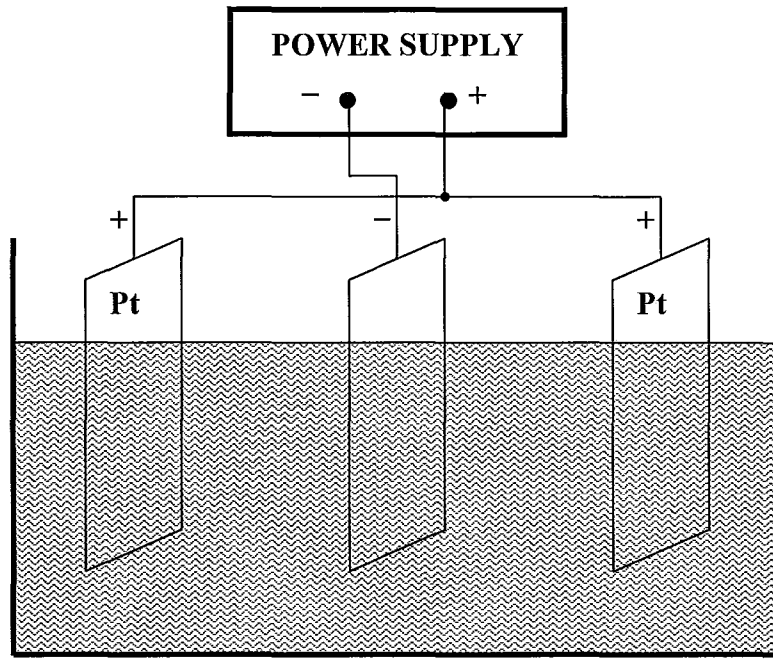

Figure 4-1 Schematic of the setup of the deposition cell

The cell included a cathodic substrate (15-30 cm^2) centered between two parallel platinum (Pt) counter electrodes. The distance between cathodes and anodes was 15 mm. The volume of the deposition bath varied from 50 to 200 ml. An electrophoresis power supply EPS 601 (Amersham Biosciences) was employed to provide the DC electric field for electrodeposition, either in a constant current density (galvanostatic) or a constant voltage mode.

4.3.1 Preparation of solutions and suspensions for electrodeposition

4.3.1.1 Preparation of solutions of chitosan and zinc acetate

3.0 gL^{-1} chitosan was dissolved in a 1% acetic acid solution, which was then used to prepare chitosan solutions containing other biomacromolecules or ceramics. The solutions with 0.5 gL^{-1} chitosan and different concentrations of zinc acetate (0~8mM) were prepared for electrolytic deposition. The aqueous solutions of chitosan and zinc acetate were stirred until completely dissolved.

4.3.1.2 Preparation of suspensions of chitosan and zinc oxide

3.0 gL^{-1} chitosan was dissolved in a 1% acetic acid solution, which was then diluted to 0.5 gL^{-1} in a mixed ethanol-water solvent (17 vol% water). These solutions with 0.5 gL^{-1} chitosan and different concentrations (0~4 gL^{-1}) of zinc oxide nanoparticles were prepared. Before the EPD, the suspensions were ultrasonicated for 1 hour to achieve a homogeneous dispersion of the zinc oxide nanoparticles.

4.3.1.3 Preparation of solutions of chitosan and hemoglobin

3.0 gL^{-1} chitosan was dissolved in a 1% acetic acid solution, which was then diluted to 1 gL^{-1} chitosan solution in deionized water. These solutions with 1 gL^{-1} chitosan and different concentrations (0.05 ~ 1 gL^{-1}) hemoglobin were prepared for EPD.

4.3.1.4 Preparation of solutions and suspensions for electrochemical testing

3.0 gL^{-1} chitosan was dissolved in a 1% acetic acid solution, which was then used to prepare chitosan solutions containing other biomacromolecules or ceramics. The solutions with 0.5 gL^{-1} chitosan and different concentrations of glucose oxidase (GOx) were prepared.

Glucose oxidase solution in deionized water of controlled concentration and volume (using micropipette) was drop casted on the coated graphite electrode (6 mm diameter).

4.3.2 Electrodeposition procedures

Cathodic and anodic composite deposits were obtained on various conductive substrates under galvanostatic or constant voltage conditions. The substrates utilized included stainless steel AISI 304 foil (50×50×0.1 mm^3), silicon wafers (10×50×0.1 mm^3), graphite plates (10×50×0.1 mm^3), and graphite rods (6 mm diameter).

The constant current density employed for the galvanostatic deposition ranged from 3 to 5 mA cm^{-2}, and a constant voltage of 5~20 V was used for the constant voltage deposition. The deposition time was varied in the range of 1-10 min to obtain deposits of different thicknesses. Obtained coatings were dried in air at room temperature.

4.4 Characterization of the coatings

4.4.1 Materials characterization methods

4.4.1.1 Investigation of deposition yield

The electrodeposition yield was studied by measuring the deposit weight of the deposited coating.

In this work, the deposit weight of a deposited coating was obtained by weighing the foil substrate before and after the deposition, followed by drying at room temperature for 24 hr.

4.4.1.2 X-ray diffraction analysis

The phase content and structure of materials was determined by X-ray diffractometry (XRD). In this work, the phase content of the deposits was determined by XRD with a diffractometer (Nicolet I2), using monochromatized Cu Kα radiation at a scanning speed of 0.5° min^{-1}. The studies were performed on films deposited on various substrates and powder samples. For the fabrication of powder samples, the deposits were scraped from the Pt electrodes and dried in air for 24 hr before the XRD analysis.

4.4.1.3 Thermogravimetric and differential thermal analysis

Thermogravimetric analysis (TGA) is an analytical technique used to determine a material's thermal stability and its fraction of volatile components by monitoring the weight change that occurs as a specimen is heated. The measurement is normally carried out in air or in an inert atmosphere, and the weight is recorded as a function of increasing temperature. In addition to weight changes, some instruments also record the temperature difference between the specimen and one or more reference pans (differential thermal analysis, DTA), which can be used to monitor the energy released or absorbed via chemical reactions or phase transformations during the heating process.

In this work, TGA and DTA were carried out using the deposits that had been scraped from the Pt electrode after deposition and dried at room temperature for 24 hr. The thermoanalyzer (Netzsch STA-409) was operated in air between room temperature and 1200 °C at a heating rate of 5 °C min^{-1}.

4.4.1.4 Scanning electron microscopy

The scanning electron microscope (SEM) is a type of electron microscope that images the morphology of sample surface by scanning it with a high-energy beam of electrons in a scan pattern. The electrons interact with the atoms that make up the image

producing signals that contain information about the sample's surface topography, composition and other properties.

The surface morphology and microstructures of the deposited coatings were studied by scanning electron microscopy using a JEOL JSM-7000F scanning electron microscope.

4.4.1.5 Fourier transform infrared spectroscopy

Fourier Transform Infrared Spectroscopy (FTIR) is an analytical technique used to identify organic (and in some cases inorganic) materials. An FTIR spectrometer simultaneously collects spectral data in a wide spectral range. This confers a significant advantage over a dispersive spectrometer which measures intensity over a narrow range of wavelengths at a time. These infrared absorption bands identify specific molecular components and structures.

In this work, the deposits removed from Pt substrates were studied by FTIR using Bio-Rad FTS-40 instrument.

4.4.1.6 Circular dichroism spectroscopy

Circular dichroism (CD) refers to the differential adsorption of left and right circularly polarized light. This phenomenon is exhibited in the absorption bands of

optically active chiral molecules. UV CD is used to investigate the secondary structure of proteins. Circular dichroism spectra were recorded on an AVIV Model 215 spectropolarimeter equipped with a Thermo-Neslab circulating bath. Water solutions of appropriate samples were placed in a 0.1 cm quartz cell fitted to a thermally controlled cell holder. Each CD spectrum was obtained at 25 °C, with a 1 nm slit width and a time constant of 5s. Data was collected from 190nm to 260nm at 1nm intervals. The results of CD measurements are expressed as MRE (mean residue ellipticity), in units of $deg \cdot cm^2 \cdot dmol^{-1}$, defined as:

$$MRE=\theta/\{[c_{BSA}/M_w]r\}, \text{ for a 0.1cm pathlength} \quad (4\text{-}1)$$

Where ellipticity θ is measured in milidegrees, c is the concentration of protein (hemoglobin) (in mg mL^{-1}), M_w is the molecular weight of protein, and r is the number of amino acid residues of protein (hemoglobin).

The concentrations of protein in the solutions were determined by absorbance at 280nm against a water blank. The complex had precipitated material and therefore it was diluted until a clear solution was obtained; then the concentration of protein in the diluted complex was obtained by absorbance.

4.4.2 Electrochemical Characterization

Sensor behaviour of the fabricated electrodes was studied using a potentiostat (PARSTAT 2273, Princeton Applied Research) controlled by a computer suing a PowerSuite electrochemical software. Electrochemical studies were performed using a standard three-electrode cell containing 0.01M Phosphate Buffer Saline (PBS), degassed with purified nitrogen gas. The working electrode surface was a graphite rod (6mm) embedded in resin. The counter electrode was a platinum gauze, and the reference electrode was a standard calomel electrode (SCE). Cyclic voltammetry studies were performed within a potential range of -0.2 ~7 V versus SCE at scan rate of 10~300 mV s^{-1}.

5 Experimental Results and Discussion

5.1 Electrodeposition of biopolymers

5.1.1 Electrodeposition of chitosan

Chitosan is a linear polysaccharide (similar to cellulose) that is obtained by deacetylation of chitin [22]. Chitosan is formally a copolymer composed of aglucosamine and N-acetylglucosamine because the deacetylation of chitin is incomplete. It should be noted that the term "chitosan" does not refer to a single well-defined structure but

various forms which differ in molecular weight, degree of acetylation, and sequence [71]. The presence of the primary amine at the C-2 position of glucosamine residues makes chitosan have an unique structure feature. There are few biopolymers like chitosan that have such a high content of primary amines, and these amines confer important functional properties.

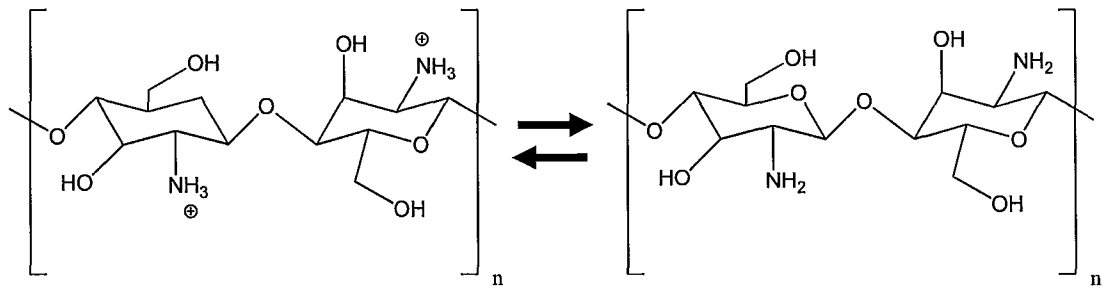

Figure 5-1 Schematic illustrating chitosan's versatility for deposition

It is shown in **Figure 5-1** that pH substantially alters the charged state and properties of chitosan. At low pH, the amines of chitosan are protonated and positively charged. The charge is attributed to protonated NH_3^+ groups. At high pH the chitosan become deprotonated and the polymer loses its charges and forms network structure which is insoluble in water. As mentioned before, the structure of chitosan can be varied ,

the soluble-insoluble transition occurs at pHs between 6 and 6.5, which is a very convenient range for biological applications [71]. At high pH, the electrostatic repulsions of chitosan macromolecules are reduced thus forming inter-polymer associations, such as, network junctions or liquid crystalline domains, which can yield films, fibers or hydrogels, depending on the conditions used to initiate the soluble-insoluble transition [71, 72].

Since chitosan can be dissolved in mildly acidic aqueous conditions, it can be readily cast into membranes and films that can be converted into insoluble networks by neutralizing the pH value. It is shown in **Figure 5-2**, that when the voltage supplied is sufficient for base generation at the cathode surface, then a localized pH gradient is formed [73]. It is suggested that the positive charge of chitosan chains is neutralized by electrogenerated OH^- in the high pH area at the electrode surface. As a result, chitosan macromolecules coagulate and form a film. However, there are no reports of the nano- and microscale morphologies of the electrodeposited chitosan [71].

Figure 5-3 shows that electrodeposited chitosan film can be varied depending on deposition conditions. When concentration of chitosan increases to 1 gL^{-1}, the deposit mass increases linearly which is in accordance with the Hamaker Equation. The decrease

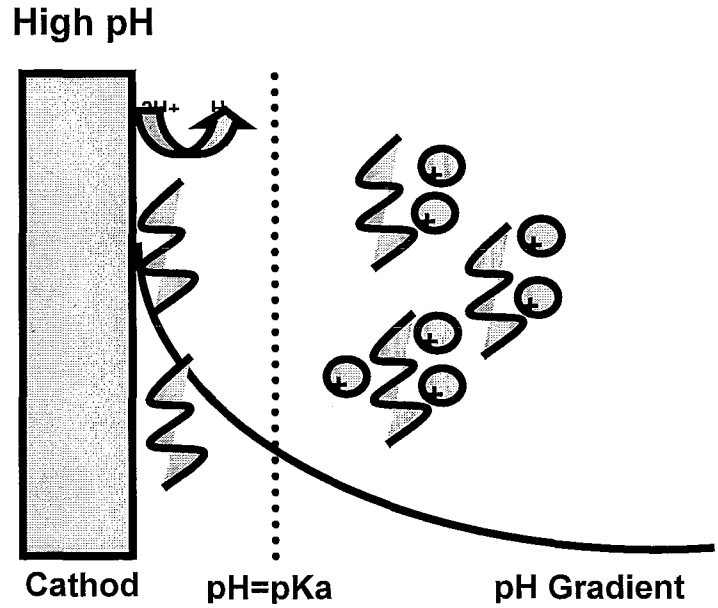

Figure 5-2 Mechanism for chitosan`s electrodeposition

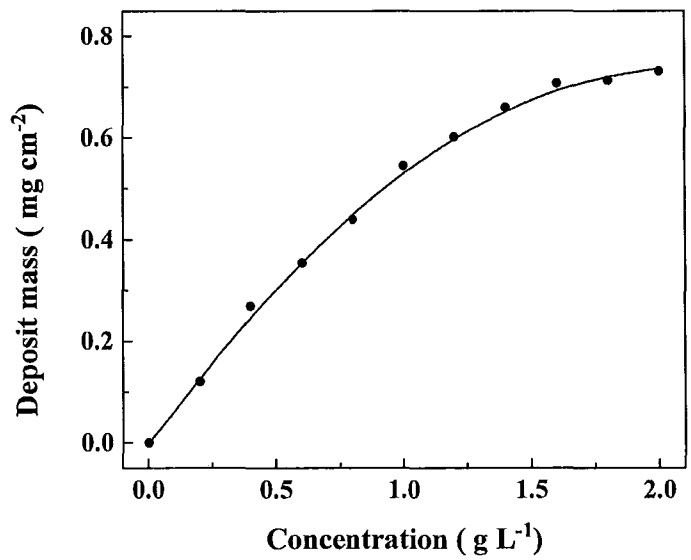

Figure 5-3 Deposit mass versus chitosan concentration in aqeous solution at constant voltage of 20V with deposition time of 2 min

of deposition rate at high concentrations can be attributed to the insulating properties of the chitosan films. Interestingly, when high current densities are imposed to generate a high localized pH, that is expected to extend further from the cathode surface, chitosan deposits as a thick hydrogel rather than a thin film [74]. It is possible to obtain thick chitosan film by increasing the deposition time at a constant voltage. In conclusion, chitosan's pH-responsive properties allow it to be electrodeposited in selective areas, and the properties of the film can be varied by changing the deposition conditions.

5.1.2 Electrodeposition of alginic acid

Alginic acid and alginates are natural biodegradable, biocompatible, non-toxic and low cost polymers, which have been utilized in many biomedical applications, such as encapsulation of drugs, cells and enzymes, and surface modification of biomedical implants [75]. The development of alginic acid coatings on stainless steel resulted in improved blood compatibility of the stainless steel implant [76].

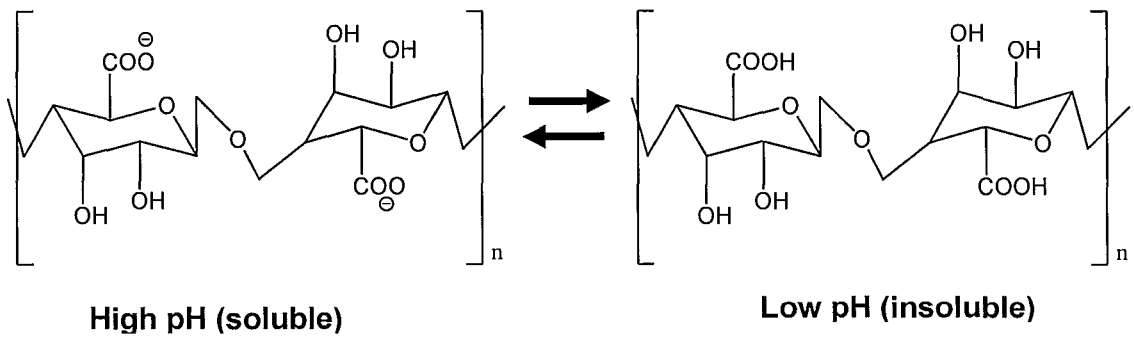

Figure 5-4 Schematic illustrating alginate's versatility for deposition

It is shown in **Figure 5-4** that pH alters the charged state and properties of alginate. At high pH, the alginate is dissociated resulting in the formation of anionic Alg^- species. At low pH, the Alg^- species formed alginic acid gel around the electrode. The mechanism for alginate electrodeposition is shown in **Figure 5-5**. Alginate is a weak polyacid with pKa =3.5. If the pH gradient is created in the presence of alginate, then alginate that experience the low localized pH at the anode surface can deposit as a gel film on the anode surface.

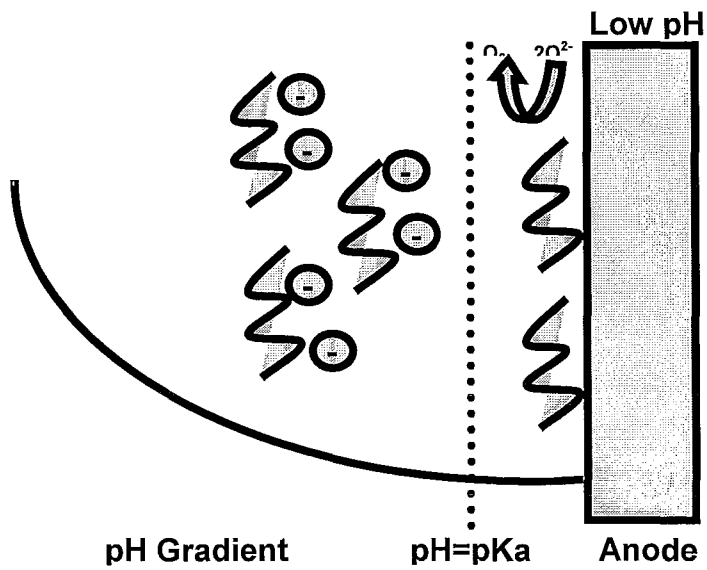

Figure 5-5 Mechanism for alginate electrodeposition

The experimental data shown in **Figure 5-6** indicates that the increase in deposit mass with increased alginate concentration is non-linear. It is in this regard that the Hamaker equation [77] predicts a linear increase in the deposit mass M with increasing particle concentration Cs in dilute solutions:

$$M = \mu E t S C_s \qquad (5\text{-}1)$$

where μ is the particle mobility in an electric field E, t is the deposition time, S is the electrode area. However, experimental data showed a non-linear increase in the deposition yield with increasing alginate concentration. This is attributed to the movement of the deposit-solution boundary during film growth [78]. **Equation 5-2** shows the deposition yield as:

$$M = \mu E t S C_s C_c/(C_c-C_s) \qquad (5\text{-}2)$$

where C_c is the alginate concentration in deposit. The Hamaker equation can be obtained when C_s is appreciably lower than C_c [78].

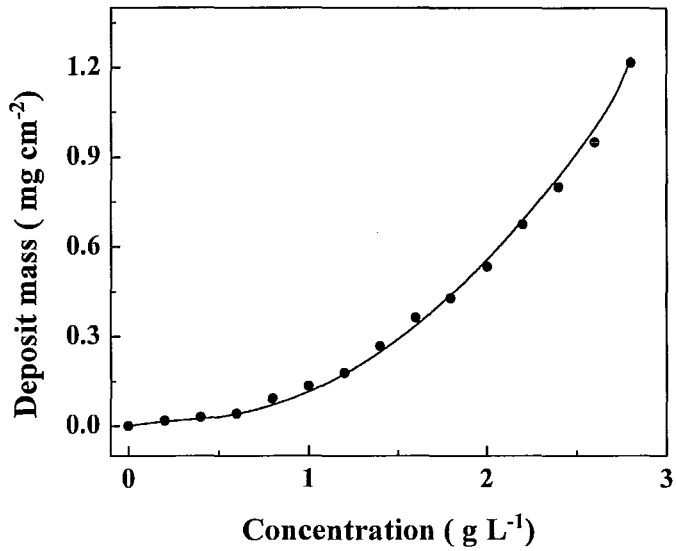

Figure 5-6 Deposit mass versus alginate concentration in aqueous solution at a constant voltage of 20V with deposition time of 2 min

5.1.3 Electrodepositon of hyaluronic acid

Hyaluronic acid (HYH) is the only non-sulfated glycosaminolglycan and is found in nearly every mammalian tissue and fluid [79]. It can be obtained from natural sources, such as rooster combs, skin, or through microbial fermentation. It is a linear polysaccharide composed of a repeating disaccharide, which are alternating residues of D-glucuronic acid and N-acetyl-D-glucosamine, as shown in **Figure 5-7** [80]. This polyanionic polymer has a range of naturally-occurring molecular sizes from 1000 to

10,000,000 Da, and has unique physicochemical properties and distinctive biological functions with applications in drug delivery and tissue engineering [81-83].

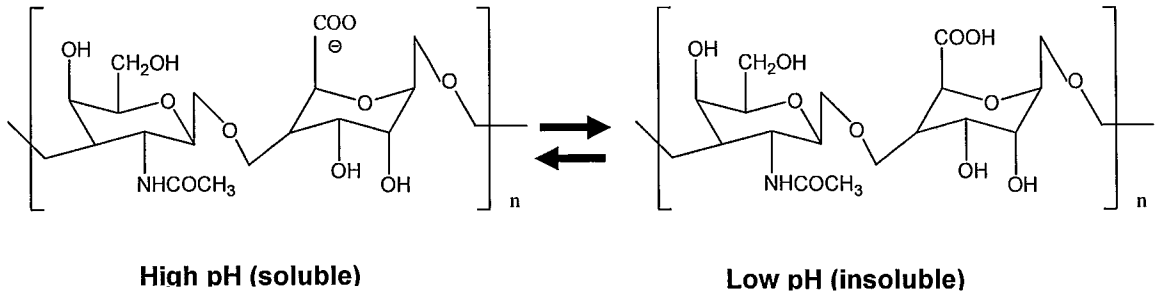

Figure 5-7 Schematic illustrating hyaluronic acid versatility for deposition

The negative charge of HYNa in solutions at pH>2.5 is attributed to the anionic –COO- groups [84]. Anodic deposits were obtained by electrodeposition from aqueous HYNa solutions as shown in **Figure 5-8**. The deposition yield increased significantly with increasing HYNa concentration.

It was suggested that the dissociation of HYNa resulted in the formation of anionic HY^- species;

$$HYNa \rightarrow HY^- + Na^+ \qquad (5\text{-}3)$$

Electric field provided electrophoretic motion of the anionic HY^- species towards the anode surface, where the pH decreased owing to the electrochemical decomposition of water (Equation (5-4)).

$$2H_2O \rightarrow O_2 + 4H^+ + 4e^- \qquad (5\text{-}4)$$

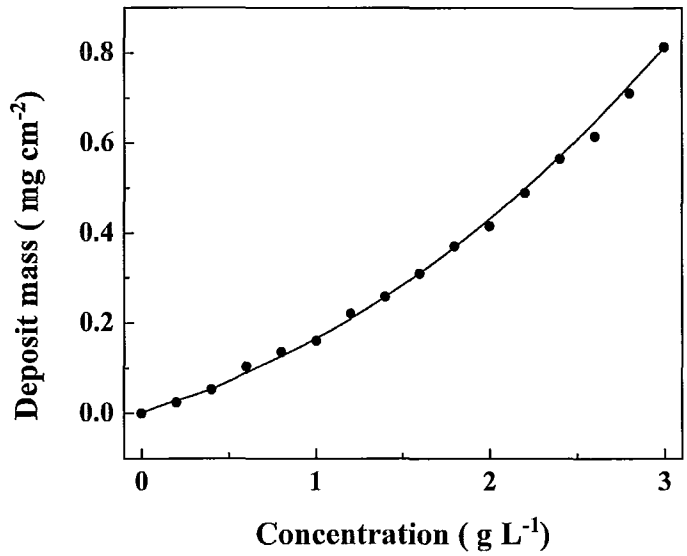

Figure 5-8 Deposit mass versus hyaluronate concentration in aqueous solution at a constant voltage of 20 V with deposition time of 2 min

The formation of hyaluronic-acid gel (HYH) in the low pH region at the electrode surface was expected as a result of the charge compensation of –COO- groups. The experimental data shown in **Figure 5-8** indicates that the dependence of deposit mass versus HYNa concentration is non-linear, which is attributed to the deposit-suspension boundary motion discussed above.

It is in this regard that the Hamaker equation [78, 85] predicts a linear increase in the deposit mass M with increasing particle concentration Cs in dilute suspensions:

$$M = \mu Et\, SC_s \qquad (5\text{-}5)$$

where μ is the particle mobility in an electric field E, t is the deposition time, S is the electrode area. However, experimental data reported showed a non-linear increase in the deposition yield with increasing ceramic particle concentration in suspensions [77].This is attributed to the movement of the deposit–suspension boundary during film growth. It was shown that the deposition yield can be described by the equation:

$$M = \mu E t\, S C_s C_c/(C_c - C_s) \qquad (5\text{-}6)$$

where C_c is the particle concentration in the deposit. When C_s is appreciably lower than C_c, the Hamaker equation can be obtained.

The more than linear curve can also be explained by depletion forces. It was illustrated that attractive ion correlation forces in the ion cloud are ignored in the Poisson-Boltzmann approximation [86]. The DLVO (Derjaguin, Landau, Verwey and Overbeek) theory can be applied for isolated pairs of particles, however, in a system with many particles, an attractive force between particles would be increased by the volume exclusion effect. This force could be significant enough to cause aggregation and flocculation of colloidal particles [87]. The DLVO theory considers only very dilute systems, in which particles contact occasionally. It should be noted that the hydrolysis of ions or complexes in electrolytic deposition and the electrophoretic motion of charged particles in suspension result in the accumulation of ceramic particles at the electrode.

Their interaction could also be influenced by ions produced or present in ELD and EPD baths [86].

5.2 Electrodeposition of composite zinc oxide – chitosan films

Various electrochemical strategies have been developed for the deposition of polymers, using cationic and anionic polyelectrolytes and charged polymer-metal ion complexes [88-93]. Chitosan is especially important for the applications in biomedical sensors, implants, microfluidic devices[78, 90, 94]. This polymer exhibits a pH-dependent positive charge in aqueous solutions. Insoluble films of chitosan can be obtained by electrochemical precipitation in the high pH area at the electrode surface. It was shown that chitosan provided dispersion and charging of inorganic nanoparticles in the suspensions and enabled electrodeposition of the composite films [78].

Electrodeposition of inorganic oxide materials can be achieved by electrosynthesis [95] or electrophoretic deposition (EPD) [96] methods. In the electrosynthesis methods, nanostructured oxide films are produced in cathodic or anodic reactions from the solutions of metal salts. Various strategies were developed for the electrosynthesis of nanostructured oxides, such as electrogenerated base method, anodic oxidation and cathodic reduction [89, 95, 97, 98]. EPD is achieved via motion of charged

particles in suspensions towards an electrode and deposit formation under an applied electric field. Cathodic or anodic deposits can be obtained depending on particle charge. Electrochemical methods have been widely investigated for the fabrication of zinc oxide films. Zinc oxide is an important semiconductor material for the application in solar cells, photovoltaic devices, batteries and biosensors [99-101].The interest in application of zinc oxide for biosensors is attributed to the high isoelectric point of this material (pH = 9.5) which is beneficial for the electrostatic immobilization of enzymes at physiological pH. Nanostructured zinc oxide was deposited by electrogenerated base method [102-105] and EPD [106, 107]. It is important to note that electrosynthesis can be used for the fabrication of thin or porous films [95]. Thick films can be deposited by EPD. However, electrophoretically deposited films exhibit low adhesion. Sintering of such films presents difficulties attributed to sintering shrinkage, cracking, chemical reactions between the deposited materials and substrates at elevated temperatures, and other factors [108].The sintering problems can be addressed by electrochemical co-deposition of zinc oxide and polymers. The use of polymers offers the advantage of low-temperature processing of composite materials.

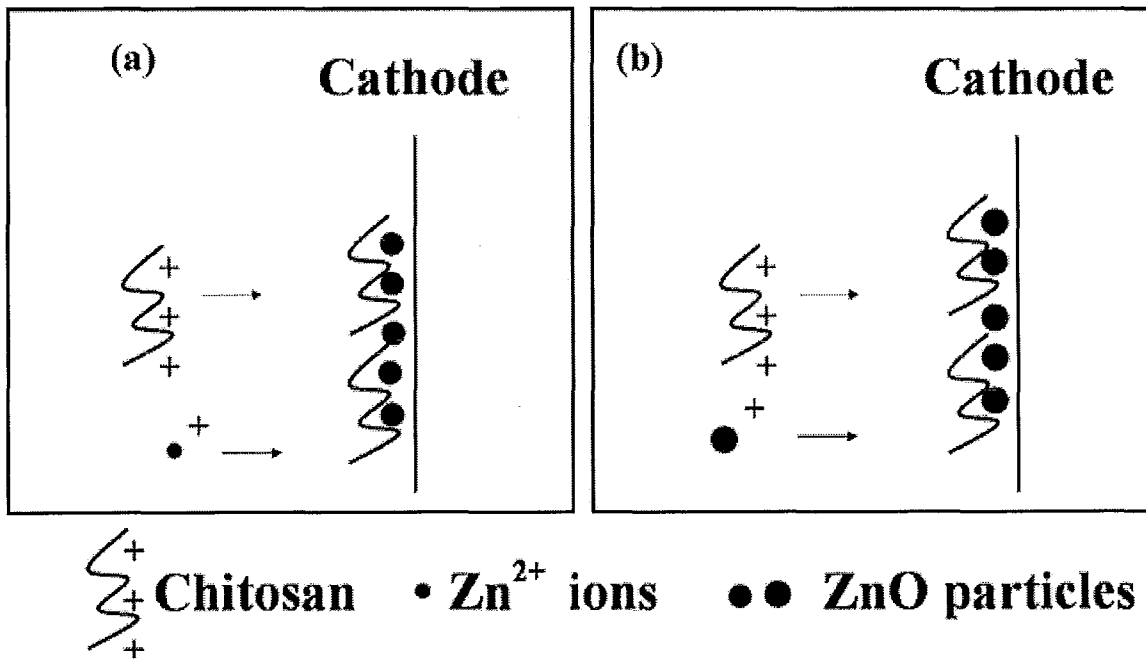

Figure 5-9 Schematic of the co-deposition mechanisms: (a) electrosynthesis of zinc oxide and EPD of CHIT (method 1), (b) EPD of zinc oxide and CHIT (method 2)

Figure 5-9 shows the schematic of the co-deposition mechanism. In method 1, the ZnO particles were synthesized from zinc acetate and CHIT solution, ZnO nanoparticles were obtained from ZnO suspension by method 2.

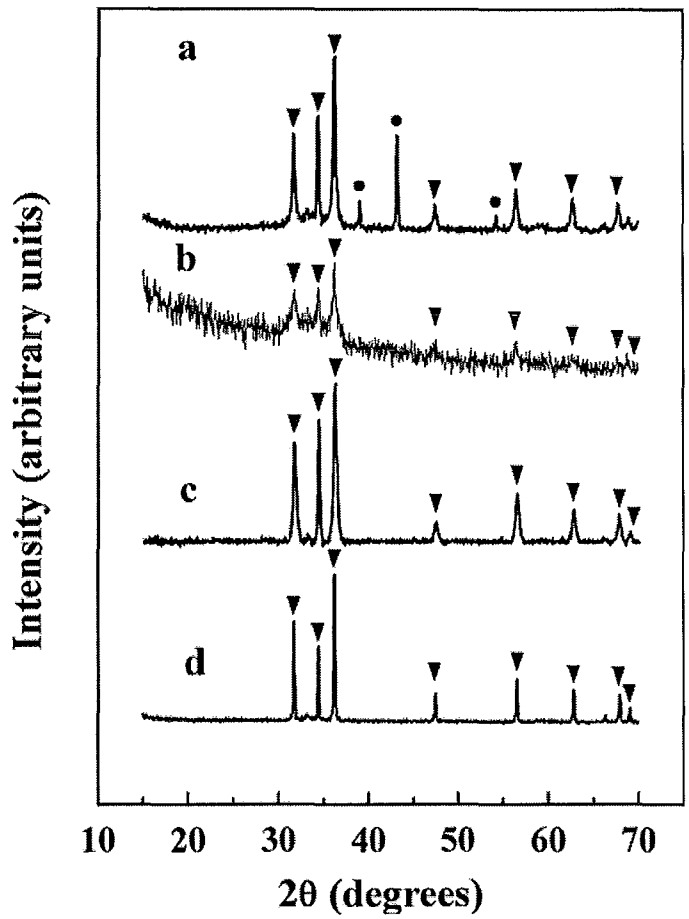

Figure 5-10 X-ray diffraction patterns for deposits prepared from (a) 5 mM aqueous zinc acetate solution, (b) 3 mM aqueous zinc acetate solution containing 0.5 gL^{-1} CH, (c) 5 mM aqueous zinc acetate solution containing 0.5 gL^{-1} CH and (d) 1.2 gL^{-1} zinc oxide and 0.5 gL^{-1} CH in a mixed water–ethanol (17% of water) solvent (▼—peaks corresponding to JCPDS file 36-1451 of zinc oxide,•—peaks corresponding to JCPDS file 4-831 of zinc metal)

Cathodic deposits were obtained from the aqueous zinc acetate solutions at 20 ◦C and investigated by XRD. The diffraction patterns **Figure 5-10** (a) showed peaks of zinc oxide (JCPDS file 36-1451) and zinc metal (JCPDS file 4-831) phases. However, the peaks of zinc metal were not observed in the diffractograms (**Figure 5-10** b and c) of the

materials prepared from CHIT solutions containing zinc acetate (method 1, **Figure 5-9** a). The XRD patterns of the deposits prepared from the 0.5 gL^{-1} CHIT solutions containing 3 mM zinc acetate showed broad peaks of zinc oxide (**Figure 5-10** b). The average particle size calculated from the X-ray broadening was found to be 15 nm. The X-ray diffraction patterns of the deposits prepared from the 0.5 gL^{-1} CHIT solution containing 5 mM zinc acetate showed sharper peaks of higher intensity (**Figure 5-10** c). The average particle size for such deposits was found to be 28 nm. The addition of zinc acetate to the 0.5 gL^{-1} aqueous CHIT solutions resulted in lower deposition rate, compared to the deposition rate obtained from pure 0.5 gL^{-1} CHIT solution. The decrease in the deposition rate was observed in the concentration range of 0~5 mM zinc acetate. The deposition rate remained nearly constant at higher concentrations (**Figure 5-11**).

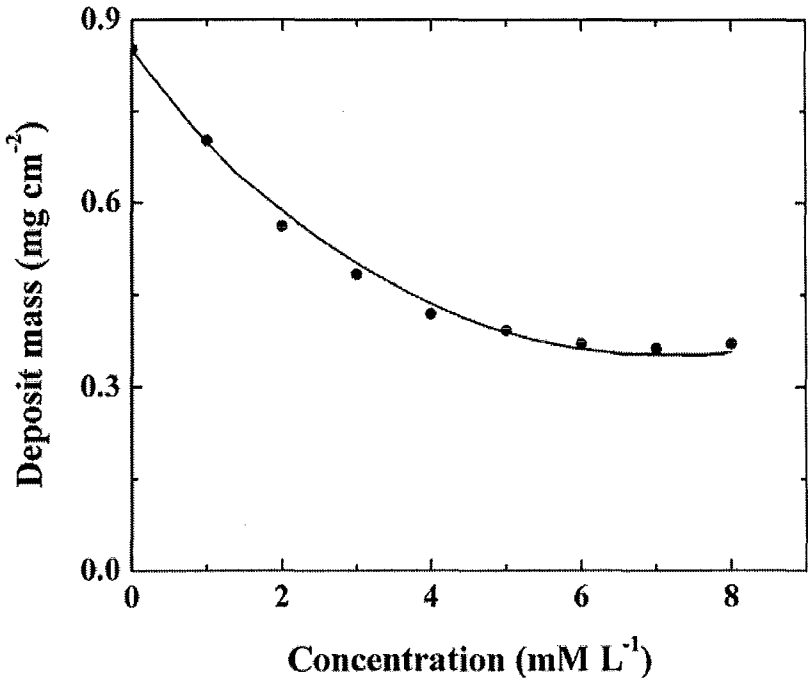

Figure 5-11 Deposit mass versus zinc acetate concentration in the 0.5 gL^{-1} CHIT solutions at a current density of 5mAcm^{-2} and deposition time of 2 min

The cell voltage increased with increasing deposition time (**Figure 5-12**). It was found that the addition of zinc acetate to the CHIT solutions resulted in lower cell voltage. **Figure 5-12** indicates that for pure 0.5 gL^{-1} CHIT solutions the cell voltage increased from 25 to 80V during 5min. However, in experiments performed at the same current density using 0.5 gL^{-1} CHIT solutions containing 5 mM zinc acetate, the voltage changed from 10 to 32V during the same deposition time.

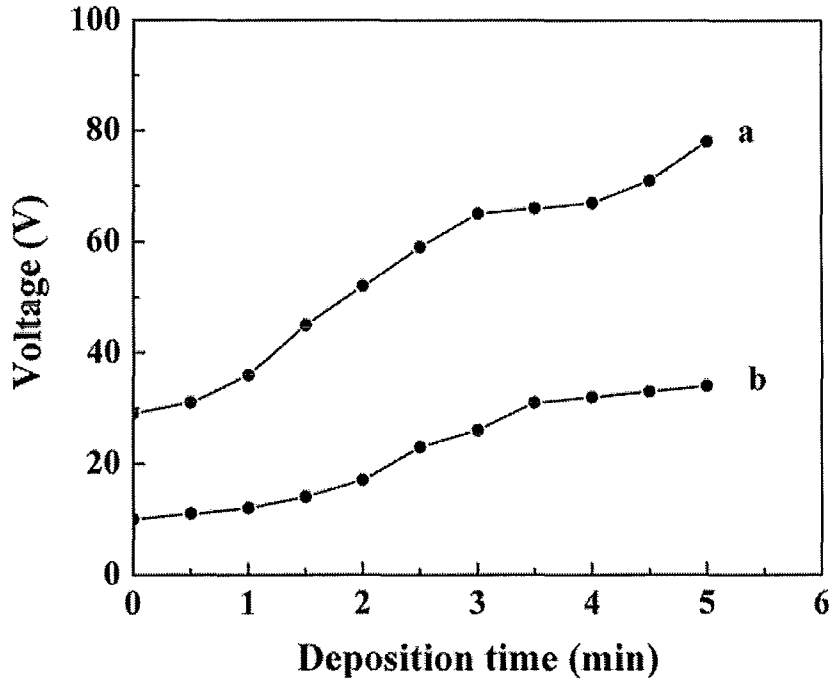

Figure 5-12 Cell voltage versus deposition time at a current density of 5mAcm^{-2} for 0.5 gL^{-1} CHIT solutions (a) without zinc acetate and (b) containing 5 mM zinc acetate

The composite films were also prepared by the combined EPD method (method 2, **Figure 5-9** b) using suspensions of commercial zinc oxide nanoparticles in a mixed water–ethanol solvent, containing dissolved CHIT. The deposition rate increased with increasing concentration of zinc oxide nanoparticles in the suspensions (**Figure 5-13**).

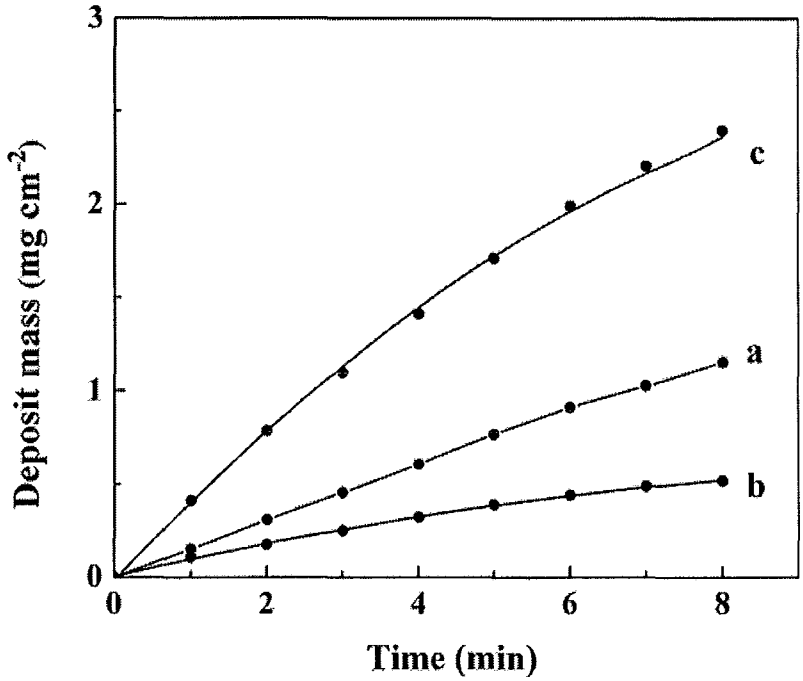

Figure 5-13 Deposit mass versus deposition time for the deposits prepared from the 0.5 gL^{-1} CHIT solutions containing: (a) 5 mM zinc acetate at a current density of 5$mAcm^{-2}$ and (b) 0.5 gL^{-1} zinc oxide, (c) 4 gL^{-1} zinc oxide at a deposition voltage of 20 V

The increase in the deposition rate can be attributed to the codeposition of zinc oxide and CHIT. The X-ray diffraction pattern of the films prepared by this method showed diffraction peaks of zinc oxide (**Figure 5-10** d). The average particle size of the zinc oxide particles calculated from the X-ray broadening was found to be 73 nm in agreement with the data provided by the zinc oxide powder manufacturer.

Figure 5-13 shows deposition yield obtained using methods 1 and 2. Film mass increased with increasing deposition time. Nearly linear dependence (**Figure 5-13** a) was obtained for the films prepared by method 1. The deposition rate decreased with time for

the film prepared by method 2. The higher concentration of zinc oxide in the suspensions resulted in a higher deposition rate (**Figure 5-13** b and c).

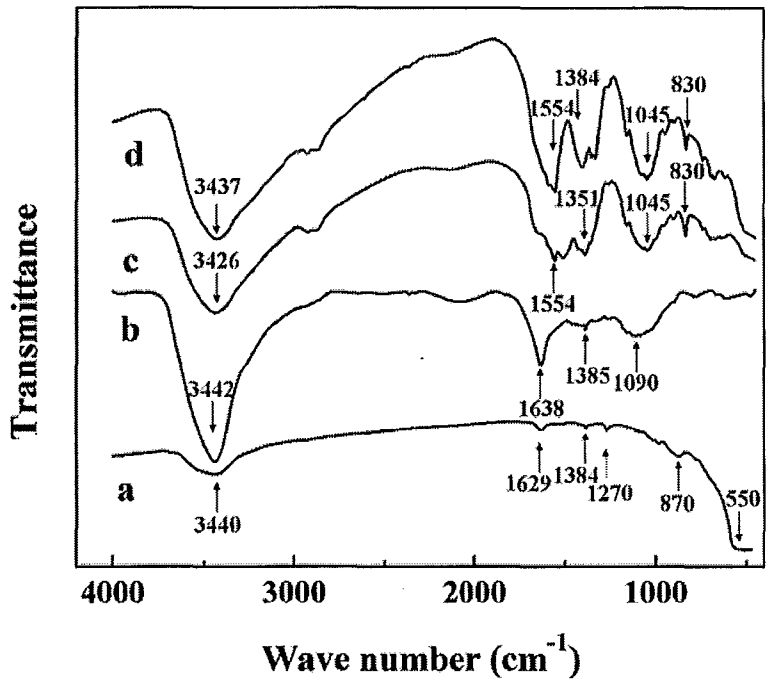

Figure 5-14 FTIR spectra for (a) zinc oxide and deposits prepared from the 0.5 gL^{-1} CHIT solutions: (b) without additives and containing (c) 5 mM zinc acetate and (d) 1.2 gL^{-1} zinc oxide

The results of the FTIR studies are shown in **Figure 5-14**. The FTIR spectrum of commercial zinc oxide powder showed a broad band below 550 cm^{-1} related to the characteristic adsorptions of zinc oxide The broad peak at ~3440 cm^{-1} can be attributed to the vibration of OH groups of adsorbed water molecules, other small peaks at 1629, 1384, 1270 and 870 cm^{-1} are related to adsorbed carbonate moieties [109-111]. The FTIR spectrum of pure CHIT deposits showed a broad peak around 3442 cm^{-1} related to hydroxyl stretching, a peak at 1638 cm^{-1} attributed to amide I stretching mode, a peak at

1385 cm^{-1} assigned to –C–O stretching mode of $–CH_2–OH$ groups and a broad peak around 1090 cm^{-1} related to C–O stretching [112, 113]. The FTIR spectra of the composite deposits showed that the peaks observed in the spectrum of pure CHIT at 1638 and 1090 cm^{-1}, shifted to 1554 and 1045 cm^{-1}, respectively. Similar shift was reported in the literature and was attributed to the formation of Zn–CHIT complexes [114, 115]. It is suggested that additional peaks at 830 cm^{-1} in the spectra of both deposits were also attributed to surface complexation [114, 115].

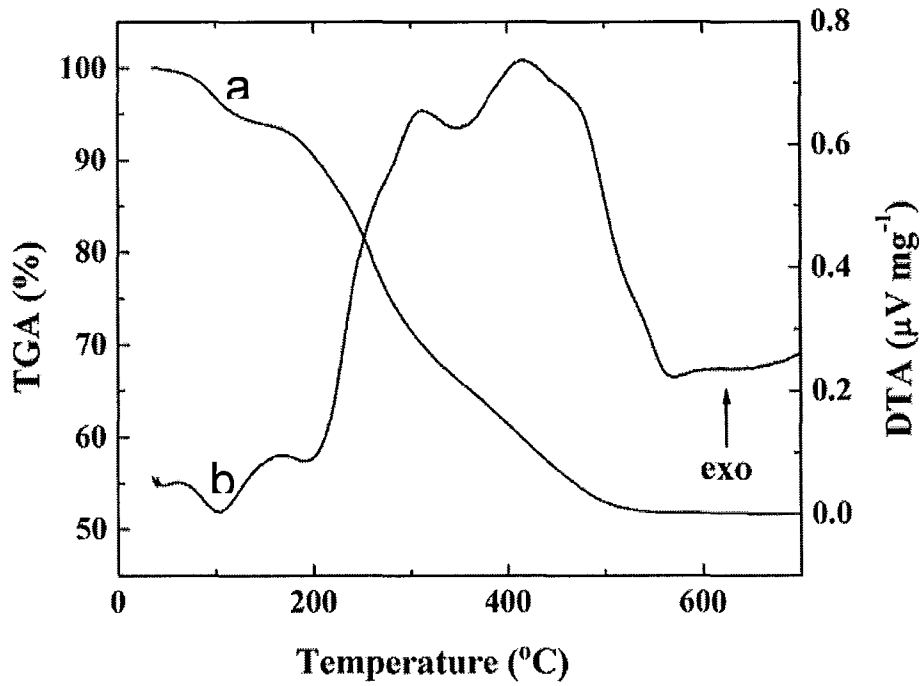

Figure 5-15 (a) TGA and (b) DTA data for composite deposits prepared from the 0.5 gL^{-1} CHIT solution containing 5 mM zinc acetate

Figure 5-15 and **Figure 5-16** show typical TGA and DTA data for the composite deposits. The TGA data (**Figure 5-15**) for the deposits prepared by method 1 from the

0.5 gL^{-1} CHIT solution containing 5 mM zinc acetate showed several steps in mass loss below ~540 °C. The mass loss at temperatures below 130 °C was mainly attributed to dehydration. The reduction in the sample mass at higher temperatures was attributed to dehydration and burning out of an organic phase. The sample mass remained nearly constant at temperatures above 540 °C. The corresponding DTA data (**Figure 5-15**) showed a broad endotherm at ~105 °C which was attributed to the dehydration. Two broad exothermic peaks observed in the range of 210–570 °C were related to burning out of an organic phase. The total mass loss at 700 °C was found to be 48 mass%. Therefore, from the TGA data, the zinc oxide content in the composite materials was found to be 52 mass%.

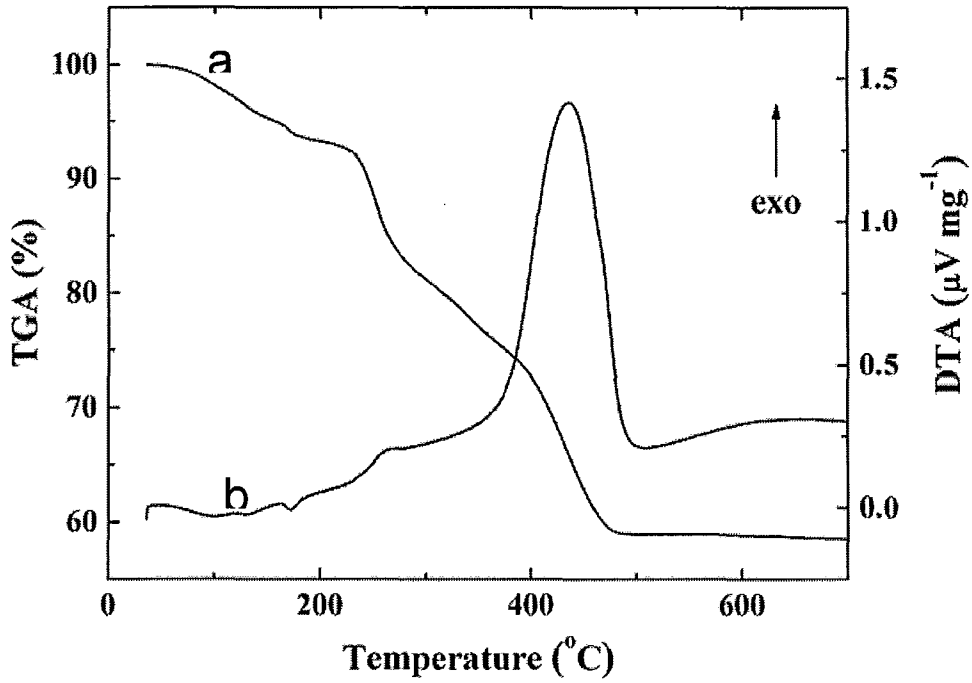

Figure 5-16 (a) TGA and (b) DTA data for composite deposits prepared from the 0.5 gL^{-1} CHIT solution containing 1.2 gL^{-1} zinc oxide

Figure 5-16 shows the TGA and DTA data for composite deposits prepared by method 2 from the 0.5 gL^{-1} CH solution containing 1.2 gL^{-1} zinc oxide. The TGA data showed steps in mass loss in the temperature range of 20~470 °C. The reduction in sample mass below ~150 °C was attributed to dehydration. Additional steps in mass loss in the range of 240~280 °C and 400~470 °C were attributed to thermal degradation and burning out of an organic phase. The corresponding DTA data (**Figure 5-16**) showed small exotherm at ~270 °C and a broad exotherm at ~450 °C attributed to burning out of an organic phase. The total mass loss at 700 °C was found to be 42 mass%. From the TGA data, the zinc oxide content in the composite deposit was found to be 58 mass%.

The experimental data presented in **Figure 5-15** and **Figure 5-16** showed that the thermal degradation of the composite material prepared by method 2 was observed at lower temperatures, compared to the composite prepared by method 1.

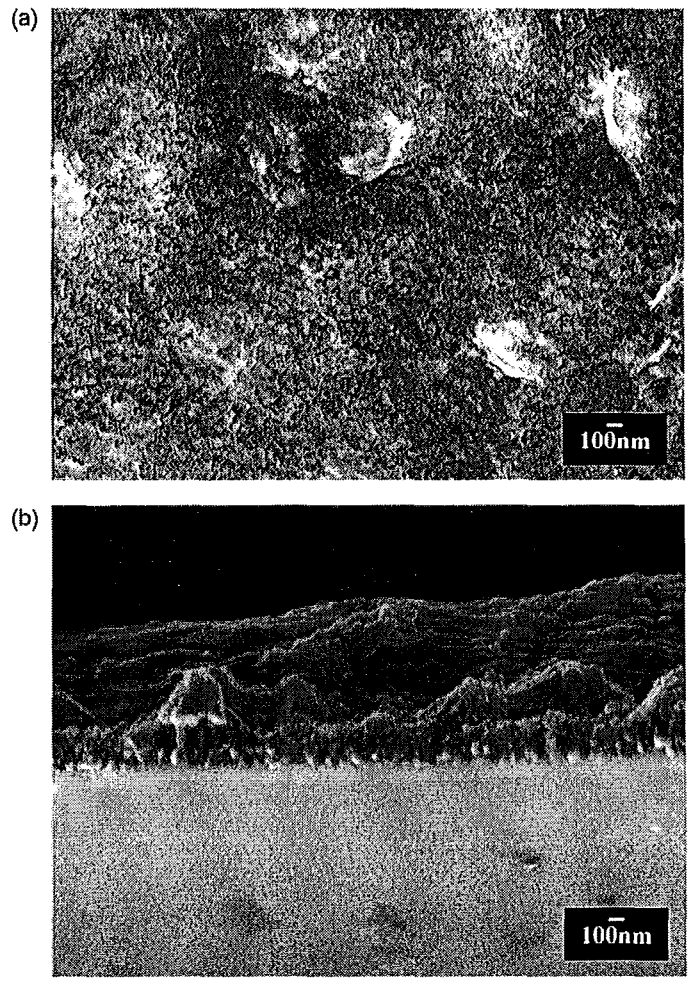

Figure 5-17 SEM image of (a) the surface and (b) cross-section of the film prepared from the 0.5 gL^{-1} CHIT solution containing 5 mM zinc acetate at a current density of 5 mA cm^{-2} and deposition time of 1 min

Figure 5-17 shows typical SEM images of the surfaces and cross sections of the films prepared by method 1. The films were relatively smooth and crack-free. The film thickness was varied in the range of 0~2 μm by the variation of the deposition time. The use of CHIT with good film forming and binding properties enabled the formation of adherent and crack-free films. The films showed porosity with pore size below 100nm(**Figure 5-17** a and b). Such porosity resulted from the cathodic gas evolution during electrodeposition.

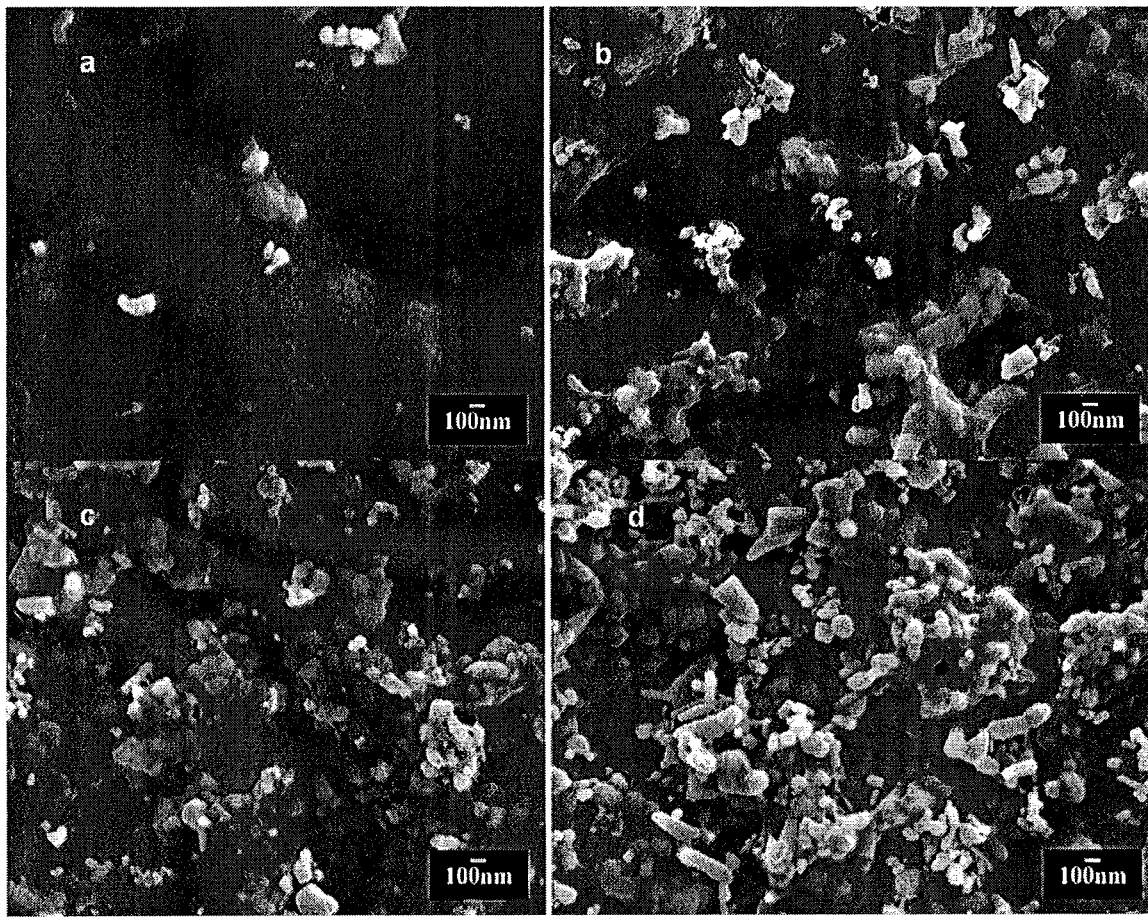

Figure 5-18 SEM images of the films prepared from the 0.5 gL^{-1} CHIT solutions containing (a) 0.4 gL^{-1}, (b) 0.8 gL^{-1}, (c) 1.2 gL^{-1} and (d) 1.6 gL^{-1} zinc oxide at a deposition voltage of 20 V

Figure 5-18 compares the SEM images of the surfaces of the films prepared by method 2, using the 0.5 gL^{-1} CHIT solutions with different concentrations of zinc oxide particles. The SEM images showed zinc oxide particles in a CHIT matrix. The increase in zinc oxide concentration in the solutions resulted in larger zinc oxide content in the composite films. The comparison of the SEM images showed that zinc oxide content in

the composite films can be varied by the variation in zinc oxide concentration in the suspensions. SEM images showed non-uniformity in zinc oxide distribution in the CHIT matrix. Some zinc oxide particles form agglomerates, containing several particles. It is suggested that CHIT can provide bridging flocculation of individual particles.

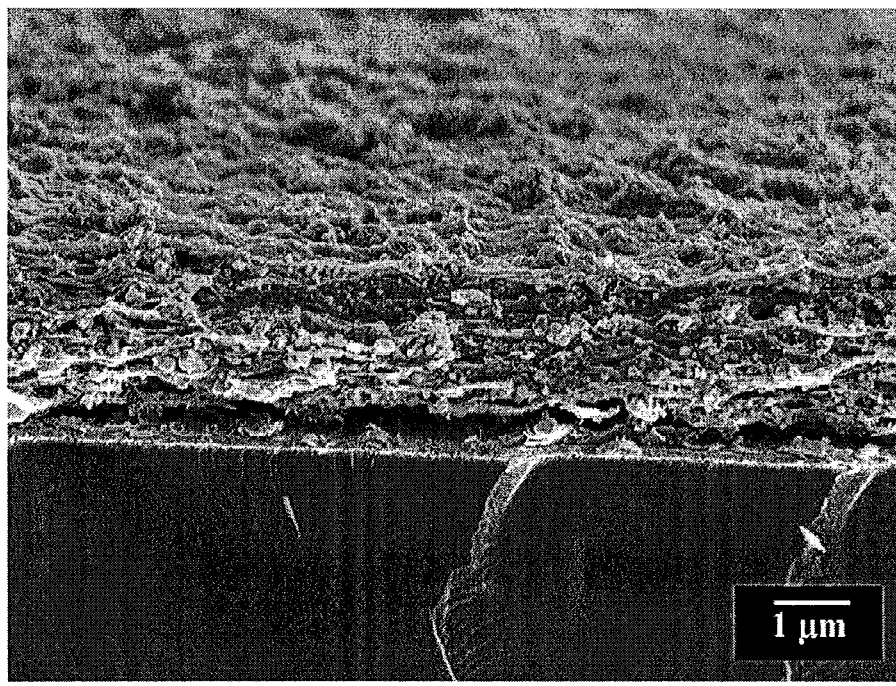

Figure 5-19 SEM image of the cross-section of the film prepared from the 0.5 gL^{-1} CHIT solution containing 1.2 gL^{-1} zinc oxide at a deposition time of 1 min and deposition voltage of 20 V

Figure 5-19 shows a cross-section of a composite film prepared by method 2. The fracture of the film showed zinc oxide particles in a CHIT matrix. The surface roughness of the film was comparable with the size of zinc oxide particles. The surface roughness of

the films prepared by method 2 was higher compared to the films prepared by method 1 due to the larger size of the zinc oxide particles. The investigation of the films prepared from the suspensions with different zinc oxide concentrations showed that film thickness can be varied in the range of 0~5 μm by the variation of the deposition time.

The results of this investigation showed that composite zinc oxide–CHIT films can be prepared electrochemically. Method 1 was based on the electrosynthesis of zinc oxide and EPD of CHIT. In method 2, EPD was utilized for the deposition of both zinc oxide and CHIT phases. The deposits prepared at 20 °C from the zinc acetate solutions without CHIT contained zinc oxide and zinc metal phases. It is in this regard that electrosynthesis of zinc oxide is usually performed at temperatures 40~70 °C from the solutions of zinc salts containing hydrogen peroxide or with oxygen bubbling [116-118] in order to avoid the deposition of zinc metal and zinc hydroxide. In contrast, electrosynthesis from the zinc acetate solutions containing CHIT resulted in the deposition of zinc oxide.

Method 1 provided the electrosynthesis of zinc oxide in situ in a CHIT matrix. The pH increase at the electrode surface was generated ele ctrochemically using the reduction reaction:

$$2H_2O + 2e \rightarrow H^2 + 2OH^- \qquad (5\text{-}7)$$

Zinc oxide precipitated at the cathode surface:

$$Zn^{2}+ +2OH- \rightarrow ZnO + H_2O \qquad (5\text{-}8)$$

The mechanism of CHIT deposition was described in the literature [62, 90, 119]. It is known that in acidic solutions the protonated CHIT becomes a cationic polyelectrolyte:

$$CHIT - NH^{2} + H_3O+ \rightarrow CHIT - NH^{3+} + H_2O \qquad (5\text{-}9)$$

However, the increase in solution pH results in a decreasing charge and at pH= 6.5 CHIT`s amino groups become deprotonated. It is suggested that electric field provided electrophoretic motion of charged CHIT macromolecules to the cathode. The pH increase at the cathode surface resulted in the formation of insoluble deposit:

$$CHIT - NH^{3+} + OH^{-} \rightarrow CHIT - NH^{2} + H_2O \qquad (5\text{-}10)$$

XRD studies showed that the size of the zinc oxide nanoparticles, prepared by the method 1, is on the nanometric scale and can be varied by variation of the zinc acetate concentration in the CH solutions. It is suggested that the formation of zinc metal phase was prevented due to the small size of the nanoparticles, which oxidized in the air. However, the polymer matrix, within which the inorganic phase is formed, plays an important role in the synthesis of the inorganic particles and determining their physical properties in addition to providing a means of particle dispersion. Previous investigations

showed the influence of polymers on the phase content and crystallinity of the inorganic nanoparticles formed by electrosynthesis in a polymer matrix [120, 121]. Nanostructured oxides were also obtained by chemical precipitation in polymer capsules without additional annealing [122]. The formation of oxide nanoparticles within the polymer matrix is influenced by diffusion limitations in the polymer matrix, local pH and interactions of metal ions and amino groups of polymer. Such local conditions and interactions can result in the dehydration of zinc hydroxide and the formation of oxide nanoparticles.

The addition of zinc acetate to CHIT solutions resulted in the formation of composite deposits, however the deposit mass decreased with increasing zinc acetate concentration (**Figure 5-11**) in the range of 0~5mM. It should be noted that in method 1, the electrosynthesis of zinc oxide and electrodeposition of CHIT required the base generation in cathodic reactions (**Eq. (5-7)**). Therefore, electrodepositionwas performed at a constant current density. The galvanostatic deposition allowed the constant rate of OH^- generation and constant deposition rate (**Figure 5-13** a). However, it is important to note that electrodeposition mechanism of CHIT involves electrophoretic motion under an influence of an electric field. The experimental data shown in **Figure 5-12** indicated that the addition of zinc acetate to the CHIT solutions resulted in lower cell voltage during

electrodeposition. The decrease in the cell voltage can be attributed to higher conductivity of the solutions containing zinc acetate. The reduction in the cell voltage resulted in a reduced electric field in the solutions and lower speed of the electrophoretic motion of CHIT macromolecules, which, in turn, resulted in the lower deposition rate of CHIT. However, the addition of zinc acetate to the CHIT solutions resulted in the deposition of zinc oxide. Therefore, no further reduction in the deposit mass was observed for zinc acetate concentrations above 5 mM.

FTIR studies (**Figure 5-14**) of the deposits prepared by methods 1 and 2 showed the formation of Zn– CHIT complexes. It was suggested that the deposition of composite zinc oxide– CHIT films resulted in the chelation of Zn and CHIT at the zinc oxide particle– CHIT interface. However, the deposits prepared by method 1 showed mass loss at higher temperatures, compared to the deposits prepared by method 2 (**Figure 5-15** and **Figure 5-16**). The difference can be attributed to the enhanced complexation of the CHIT matrix in the composite materials prepared by method 1. It is suggested that smaller particle size of the zinc oxide particles prepared by method 1 resulted in a higher surface area and enhanced surface complexation of organic and inorganic components, which, in turn, resulted in different thermal behaviour of the composite films. It is known that CHIT exhibits relatively high binding capacity (~80mg of zinc per 1 g of CHIT). The Zn

chelated CHIT showed thermal degradation at higher temperatures compared to pure CHIT [123]. The chelation can also be expected in the electrodeposition bath, which contained Zn^{2+} ions and CHIT. The extent of binding of the ions by polymer depends on the concentration of metal ions in solutions, polymer concentration, pH and other factors [89]. The pH value is a very important factor in polymer binding since protons and metal ions compete to be bound to the polymer. It is known that the binding capacity increases with increasing pH [89]. Therefore, the formation of CHIT –metal ion complexes can be enhanced in the high pH region at the cathode surface [89].

Electrophoretic co-deposition allowed the formation of composite deposits from the suspensions of commercial ZnO nanoparticles in CHIT solutions by method 2. Mixed ethanol–water solvent was used for the deposition. The use of ethanol as a solvent offers the advantage of reduced gas evolution. However, the deposition of CHIT required certain amount of water for OH^- generation. Therefore, mixed ethanol–water solvent was used for the deposition. EPD was performed at constant voltage conditions in order to provide sufficient electric field for the deposition of zinc oxide particles and CHIT. It should be noted that method 2 enabled the formation of thicker films, compared to the method 1. It is in this regard that electrosynthesis of zinc oxide in the method 1 requires electrochemical reactions at the electrode surface. The formation of films with low

conductivity decreases the charge transfer and limits the film thickness. In contrast, in method 2, zinc oxide particles were deposited by EPD, which does not require charge transfer and enables the formation of thicker films. It is in this regard that this method enabled the formation of thick deposits of insulating materials with typical thickness in the range of 10–1000 μm [96]. It is known that isoelectric point of zinc oxide is 9.5 [101]. Therefore, electrostatic repulsion of the protonated CHIT and zinc oxide can be expected in the acidic solutions used for deposition. It is known that polyelectrolytes exhibit significant non-electrostatic interactions with oxide surfaces [62]. Therefore, the adsorption of CHIT on the zinc oxide particles can be expected in the bulk of the suspensions. Such adsorption can be related to the formation of the Zn– CHIT chelates at the zinc oxide– CHIT interface. It is suggested that the reduction in the electrostatic repulsion in the high pH region at the electrode surface promoted the chelation in the deposited films.

The deposition yield measurements showed an increase in the deposit mass with increasing zinc oxide concentration in the suspensions. Such increase can be attributed to the increasing deposition rate of zinc oxide. Indeed, SEM investigations (**Figure 5-18**) showed that the increase in zinc oxide concentration in the suspension resulted in the increase in zinc oxide content in the deposits. The deposition yield measurements

coupled with the results of SEM investigations showed that the amount of the deposited material can be varied. The decrease in the deposition rate with time is attributed to the increase in voltage drop across the deposited layer and corresponding decrease in the electric field in the bulk of the suspension [124, 125]. The deposits prepared by method 2 contained commerci al zinc oxide powders with average particle size o f ~73 nm. In contrast, electrosynthesis of zinc oxide in situ in a CH matrix (method 1) resulted in smaller particles, the size of the particles can be varied. The results of this investigation showed the possibility of electrochemical deposition of zinc oxide– CHIT composite films. Such films are promising materials for the fabrication of biosensors. It is in this regard that zinc oxide– CHIT films prepared by other methods were successfully used for the immobilization of enzymes and fabrication of efficient biosensors [100, 101].

5.3 Electrodeposition of biopolymers with enzymes

5.3.1 Electrodeposition of biopolymers with glucose oxidase (GOx)

Glucose oxidase (GOx) is used in the fields of food and fermentation industry apart from being an analytical tool in environmental monitoring and biosensors for medical applications [126-129]. GOx can not be deposited on the substrate by electrodeposition directly because of the charge reversal at the electrode surface.

However, co-deposition of GOx and biopolymers resulted in the formation of composite films.

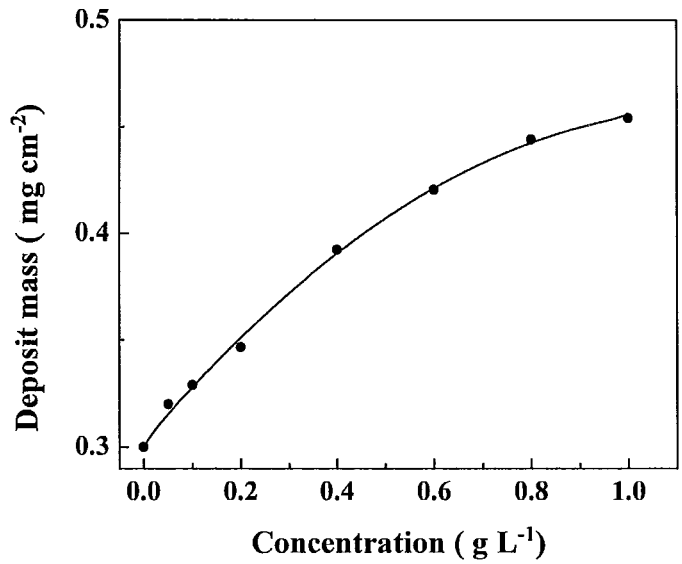

Figure 5-20 Deposit mass versus glucose oxidase concentration in the 0.5 gL^{-1} chitosan solutions at a deposition voltage of 20 V and deposition time of 2 min

Figure 5-20 shows deposit mass versus GOx concentration in 0.5 gL^{-1} chitosan solution at a constant voltage of 20 V and deposition time of 2 min. The increase in GOx concentration in the solution resulted in an increasing deposit mass, indicating the formation of composite chitosan-GOx films with different GOx contents. The decrease of the deposition rate can be attributed to formation of dense insulating films.

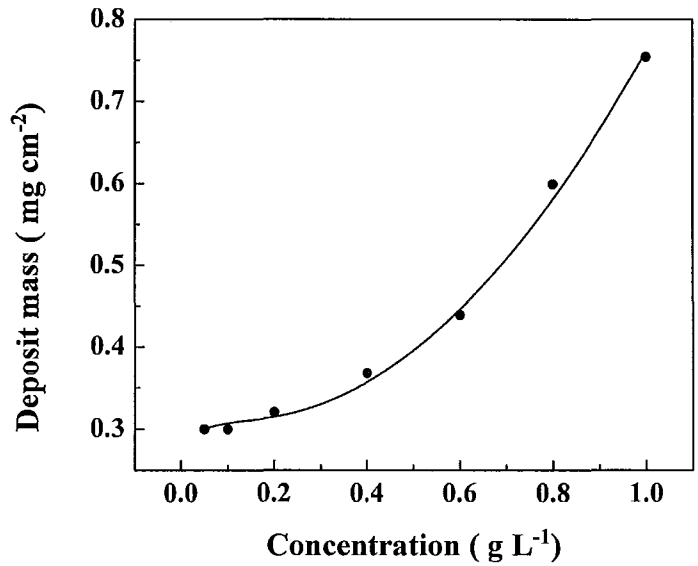

Figure 5-21 Deposit mass versus glucose oxidase concentration in the 1 g L^{-1} alginate solutions at a deposition voltage of 20 V and deposition time of 2 min

Figure 5-21 shows deposit mass versus GOx concentration in the 1 gL^{-1} alginate solutions at a constant voltage of 20 V with deposition time of 2 min. The deposit mass goes up significantly with the increase of the GOx concentration, which can be attributed to the deposit- suspension boundaries motion and enhanced coagulation due to the depletion forces [89]. **Figure 5-22** shows deposit mass versus GOx concentration in the 1 g L^{-1} hyaluronate solutions at a constant voltage of 15 V and deposition time of 2 min. Similarly, the deposit mass increases with the increase of the GOx concentration in the hyaluronate solutions.

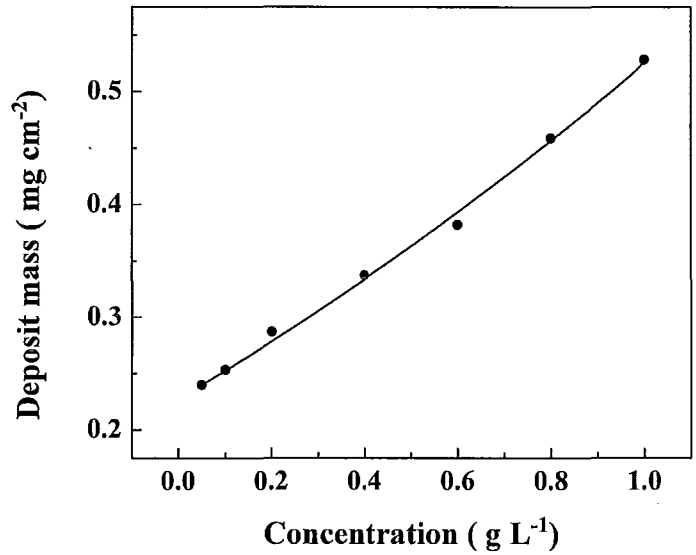

Figure 5-22 Deposit mass versus glucose oxidase concentration in the 1 gL^{-1} hyaluronate solutions at a deposition voltage of 15 V and deposition time of 2 min

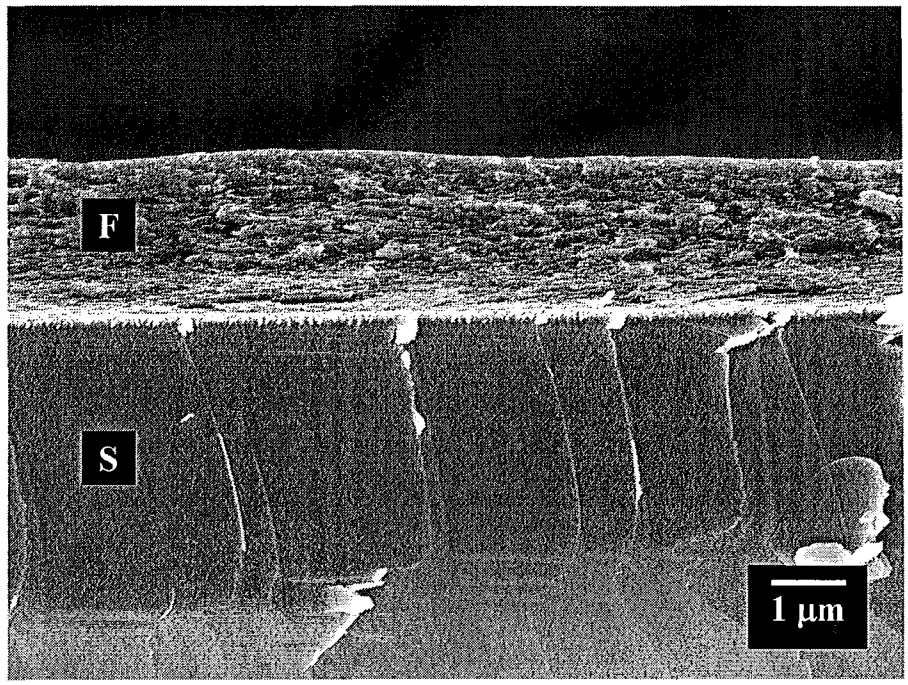

Figure 5-23 SEM image of the cross-section of the film prepared from the 0.5 gL^{-1} chitosan solutions containing 1 gL^{-1} glucose oxidase at a deposition voltage of 20 V and deposition time of 6 min

Figure 5-23 shows SEM image of complex chitosan- GOx films. Relatively uniform film was obtained at a deposition voltage of 20 V and deposition time of 6 min. The thickness was about 2 μm.

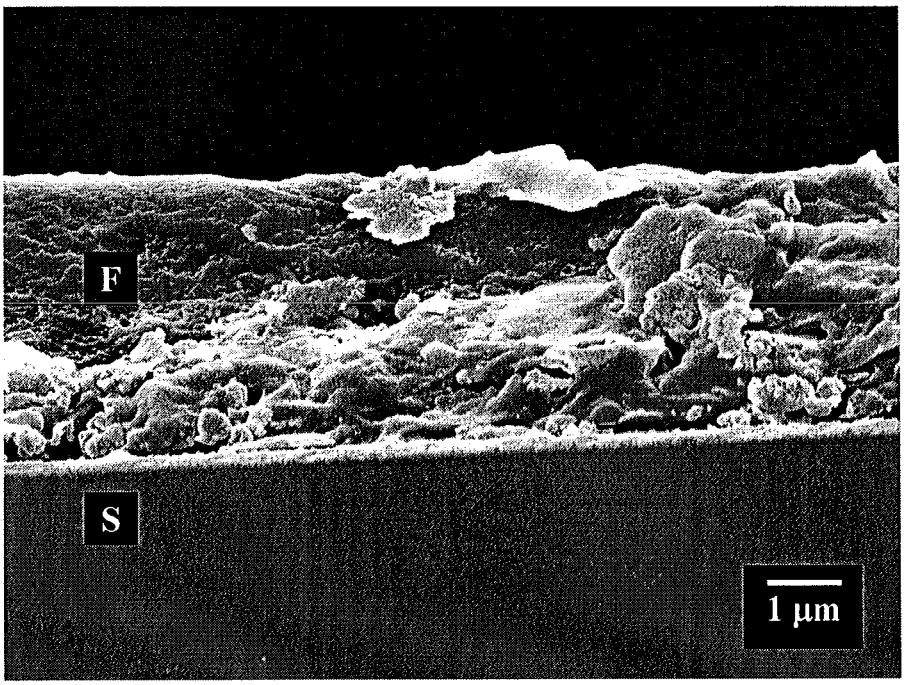

Figure 5-24 SEM image of the cross-section of the film prepared from the 1 gL^{-1} alginate solutions containing 1 gL^{-1} glucose oxidase at a deposition voltage of 20 V and deposition time of 6 min

Figure 5-24 and **Figure 5-25** show the SEM image of the cross-section of the film prepared from the 1 gL^{-1} alginic solutions containing 1 gL^{-1} GOx and SEM image of the cross-section of the film prepared from the 1gL^{-1} hyaluronate solutions containing 1g L^{-1} GOx respectively. The film showed good adhesion between GOx-alginic acid complex and silicon wafer.

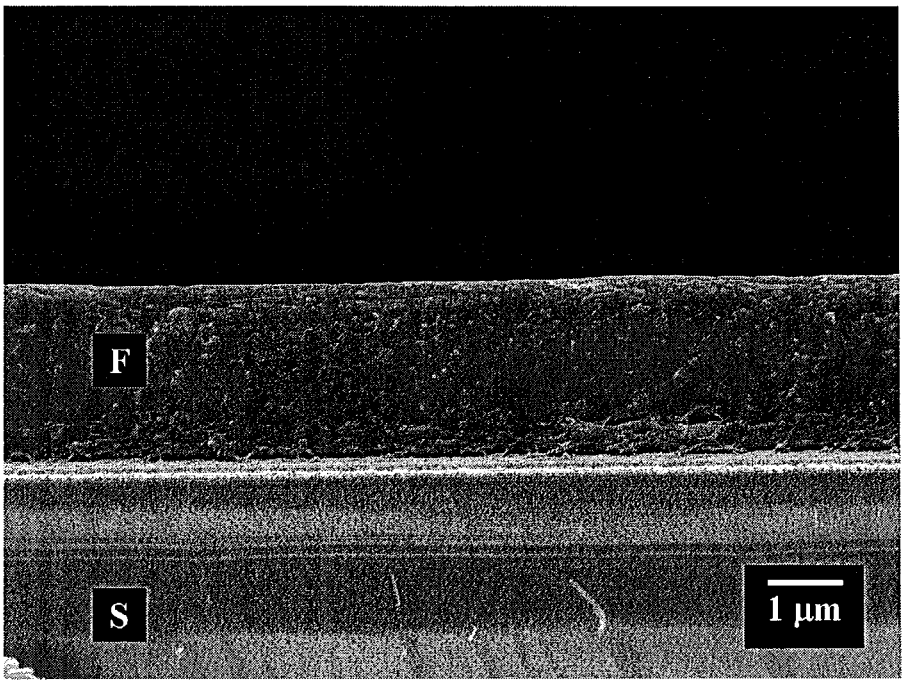

Figure 5-25 SEM image of the cross-section of the film prepared from the 1 g L^{-1} hyaluronate solutions containing 1 g L^{-1} glucose oxidase at a deposition voltage of 20 V and deposition time of 6 min

Figure 5-25 shows the SEM image of the cross-section of the film prepared from the 1gL^{-1} hyaluronate solutions containing 1gL^{-1} glucose oxidase at a deposition voltage of 20 V and deposition time of 6 min. The film was relatively smooth and crack-free, the thickness was relatively uniform and can be varied in the range of 1~ 3 μm by variation of deposition parameters, such as deposition time and applied voltage.

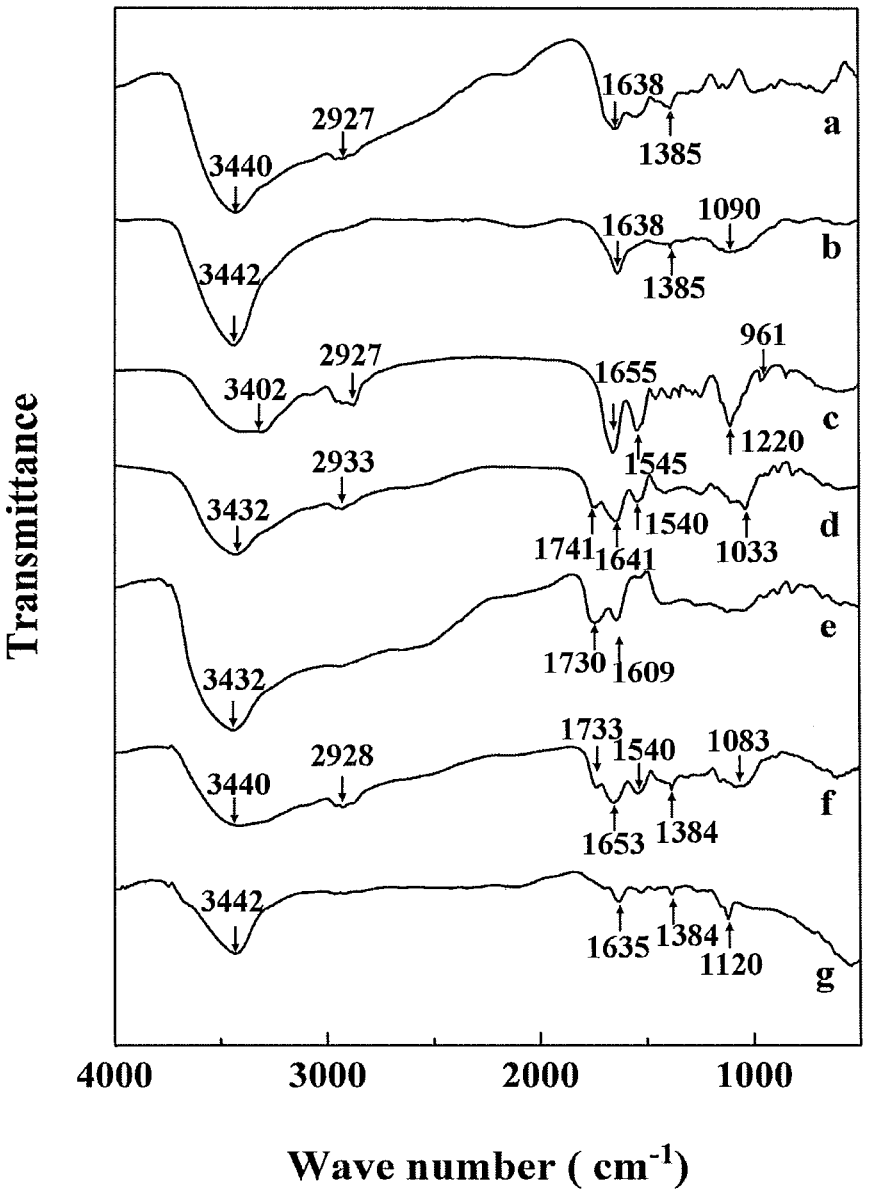

Figure 5-26 FTIR spectra for (a) deposits prepared from 0.5 gL^{-1} chitosan solution containg 1 gL^{-1} glucose oxidase, (b) pure chitosan, (c) glucose oxidase, (d) deposits prepared from 1 gL^{-1} alginic solution containg 1 gL^{-1} glucose oxidase, (e) alginic acid, (f) deposits prepared from 1 gL^{-1} hyaluronic solution containg 1 gL^{-1} glucose oxidase, (g) hyaluronic acid

The FTIR spectrum of Glucose oxidase (**Figure 5-26** c) shows absorption peaks at 2927 cm^{-1} attributed to C-H stretching, 1655 cm^{-1} for NH^{+}_{3} asymmetric bending, 1545 cm^{-1} for N-H bending [130] and the band around 1105 cm^{-1} was ascribed to bending vibrations of methyl and methylene groups and aromatic rings in GOx [131]. The FTIR spectrum of pure chitosan (**Figure 5-26** b) deposits showed a broad peak around 3442 cm^{-1} related to hydroxyl stretching, a peak at 1638 cm^{-1} attributed to C=O (amide I) stretching mode, a peak at 1385 cm^{-1} assigned to –C–O stretching mode of $–CH_2–OH$ groups and a broad peak around 1090 cm^{-1} related to C–O stretching [113, 132]. The FTIR spectrum of the composite deposits (**Figure 5-26** a) not only exhibits the characteristic absorption peak of GOx (2927 cm^{-1}), but also shows the characteristic absorption peaks of pure GOx at 1545 cm^{-1} and 1105 cm^{-1} [133], which were shifted to 1540 cm^{-1} and 1118 cm^{-1} , respectively. It is suggested that the structure of the GOx immobilized in the chitosan matrix has been changed. This is attributed to the interaction of GOx with chitosan [133].

In the FTIR spectrum of alginic acid (**Figure 5-26** e), the strong bands at 1730 cm^{-1} and 1609 cm^{-1} are related to the C=O stretching of protonated carboxylic group of alginic acid [134]. The FTIR spectrum of the film prepared from 1 gL^{-1} alginic solution containing 1 gL^{-1} GOx (**Figure 5-26** d) showed a similar band at 1741 cm^{-1} which was

attributed to C=O stretching. The additional bands at 1643 cm^{-1} and 1540 cm^{-1} can be assigned to amide I and amide II bands of GOx, respectively. The peaks at 2933 cm^{-1} and 1105 cm^{-1} due to the –C–H stretching and vibration in GOx were observ ed in spectrum of composite in agreement with literature data [130].

In FTIR spectrum of hyaluronic acid (**Figure 5-26** g), the band 1706 cm^{-1} is related to the stretching of the protonated carboxylic group of hyaluronic acid [5, 135]. The spectrum of film prepared from 1 gL^{-1} hyaluronic acid solution containing 1 gL^{-1} GOx (**Figure 5-26** f) showed additional peak at 2928 cm^{-1} , 1540 cm^{-1} and 1123 cm^{-1} which can be attributed to –C–H stretching, amide II and methylene groups of GOx, respectively.

In conclusion, the characteristic absorption peaks (2927 cm^{-1}, 1540cm^{-1} and 1105 cm^{-1}) of GOx were found in all FTIR spectra of the films prepared from solutions with 1 gL^{-1} GOx and chitosan, alginate or hyaluronate. This fact indicated that GOx was effectively immobilized on the films of chitosan, alginic acid and hyaluronic acid [131].

5.3.2 Electrodeposition of biopolymers with hemoglobin

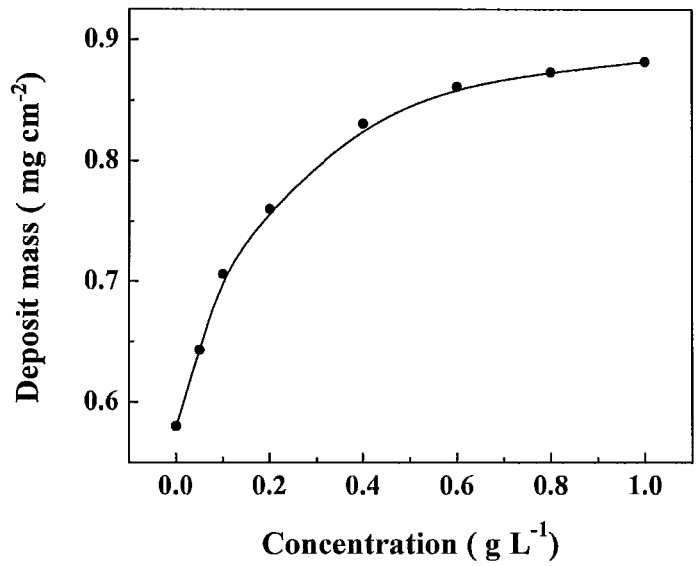

Figure 5-27 Deposit mass versus hemoglobin concentration in the 1 gL^{-1} chitosan solutions at a deposition voltage of 20 V and deposition time of 2 min

Figure 5-27 shows deposit mass versus hemoglobin concentration in 1 gL^{-1} chitosan solutions at a deposition voltage of 20 V and deposition time of 2 min. The increase in hemoglobin concentration in the 1 gL^{-1} CHIT solutions resulted in an increasing deposit mass, indicating the formation of composite chitosan-hemoglobin films with different hemoglobin contents.

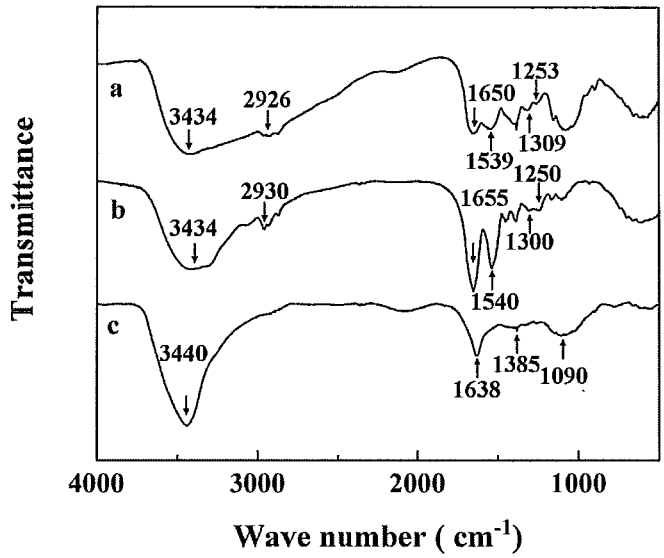

Figure 5-28 FTIR spectra for (a) deposits prepared from 1 gL^{-1} chitosan solution containg 1 gL^{-1} hemoglobin (b) hemoglobin (c) chitosan

The FTIR spectrum of pure chitosan (**Figure 5-28** c) deposit showed a broad peak around 3440 cm^{-1} related to hydroxyl stretching, a peak at 1638 cm^{-1} attributed to C=O (amide I) stretching mode, a peak at 1385 cm^{-1} assigned to –C–O stretching mode of $–CH_2–OH$ groups and a broad peak around 1090 cm^{-1} related to C–O stretching [112, 113]. The spectrum of hemoglobin (**Figure 5-28** b) has two major bands: the first band at 1655 cm^{-1} arising from the amide C=O (amide I), and the second band at 1540 cm^{-1} is related to the N-H bending (the amide II band) vibrations of peptide groups in proteins [136]. The bands at 1454 cm^{-1} and 1388 cm^{-1} arise from the bending vibrations of $–CH_2$

and $-CH_3$ groups of amino acids in the protein side chains [136]. The bands around 2930 cm^{-1} are the symmetric and asymmetric $-CH_2$ and $-CH_3$ stretching vibrations from protein side chains. The characteristic bands at 1300 cm^{-1} and 1250 cm^{-1} are attributed to N-H stretching of amide III [137]. In the FTIR spectrum of composite deposits of chitosan and hemoglobin (**Figure 5-28** a), the band around 2930 cm^{-1} can be assigned to C-H stretching which can be found in spectrum of hemoglobin (**Figure 5-28 b**). In addition, the absorption bands of the amide I (1650 cm^{-1}) , amide II (1539 cm^{-1}) and amide III (1309 cm^{-1} and 1253 cm^{-1}) of hemoglobin immobilized on chitosan are nearly the same as those of the pure hemoglobin (1655 cm^{-1} , 1540 cm^{-1} , 1300 cm^{-1} , 1250 cm^{-1}) [138]. These results indicated that hemoglobin immobilized in chitosan matrix retained its native structure and biological activity [138].

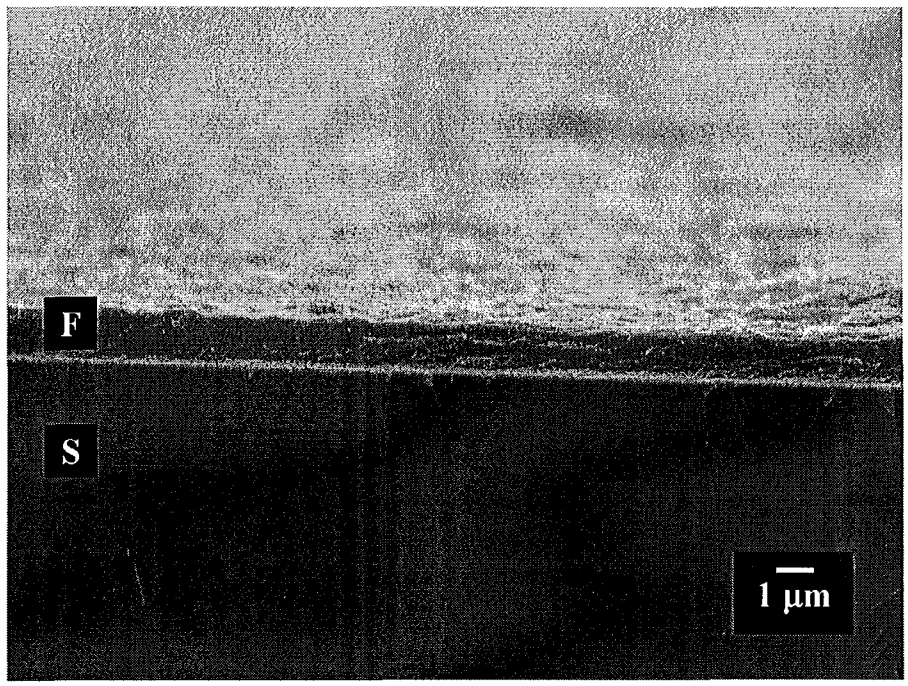

Figure 5-29 SEM image of the cross-section of the film prepared from the 1 gL^{-1} chitosan solutions containing 1 gL^{-1} hemoglobin at a deposition voltage of 20 V and deposition time of 5 min

Figure 5-29 shows SEM image of the cross-section of the film prepared from the 1 gL^{-1} chitosan solutions containing 1 gL^{-1} hemoglobin at a deposition voltage of 20 V and deposition time of 5 min. The film was relatively uniform,crack free and adherent to the substrate as shown in the SEM picture.

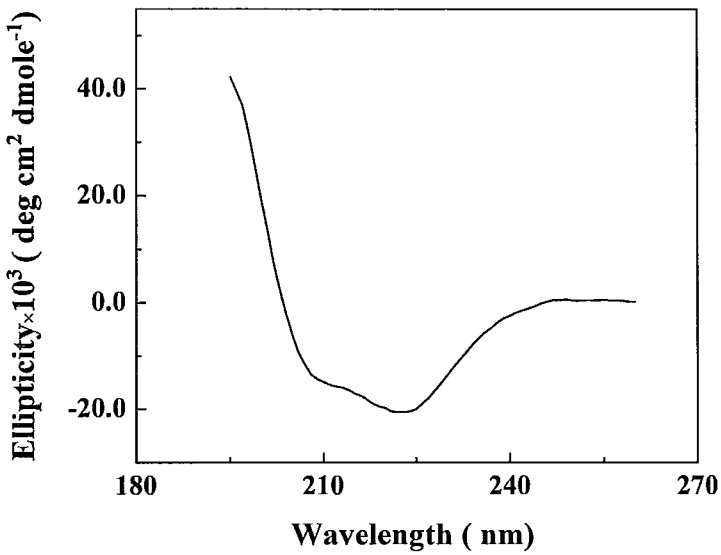

Figure 5-30 Circular dichroism spectrum of 0.03 gL^{-1} hemoglobin solution

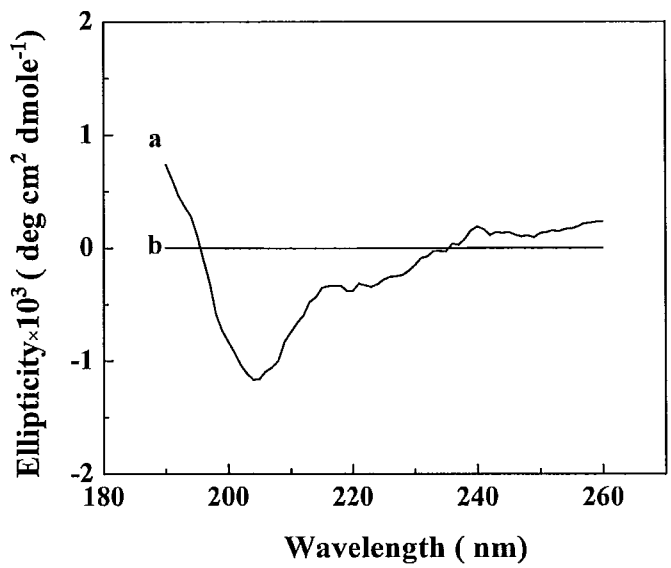

Figure 5-31 Circular dichroism spectra of (a) dissolved deposit, prepared from 1 gL^{-1} chitosan-1 gL^{-1} hemoglobin solutions (b) pure 0.03 gL^{-1} chitosan solution

Figure 5-30 and **Figure 5-31** show the circular dichroism (CD) spectra of hemoglobin (**Figure 5-30**) , chitosan (**Figure 5-31** b) and deposit prepared from 1 gL^{-1} chitosan and 1 gL^{-1} hemoglobin solution (**Figure 5-31** a). CD spectra of the samples were measured by monitoring the changes of the signal from 190 nm to 260 nm. The CD spectra of pure hemoglobin (**Figure 5-30**) shows a peak around 220 nm which can be attributed to the α–helical content of the hemoglobin [139]. For CD spectra of pure chitosan, no peaks was obtained because of no circular dichroism behaviour for the polymer. The peak around 215 nm in the CD spectra of deposit (**Figure 5-31** a) was attributed to the helix structure of the hemoglobin, thus it can be concluded that hemoglobin was immobilized in the chitosan matrix.

5.4 Electrochemical testing of fabricated electrodes

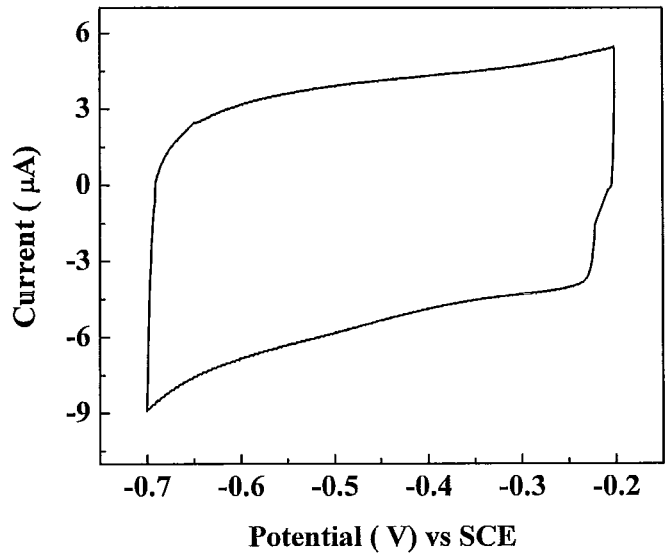

Figure 5-32 Cyclic voltammograms of the bare graphite electrode surface (diameter=6mm) in phosphate buffered saline solution (PBS) at pH 7.4 at the scan rate of 100 mV s^{-1}

The redox behavior of the electrode was investigated using cyclic voltammetry and chronoamperometry. **Figure 5-32** shows cyclic voltammograms of the bare graphite electrode surface (diameter= 6mm) in phosphate buffered saline solution (PBS) at pH 7.4 at the scan rate 100 mV s^{-1}. As can be seen, the unmodified electrode exhibited a featureless voltammetric response.

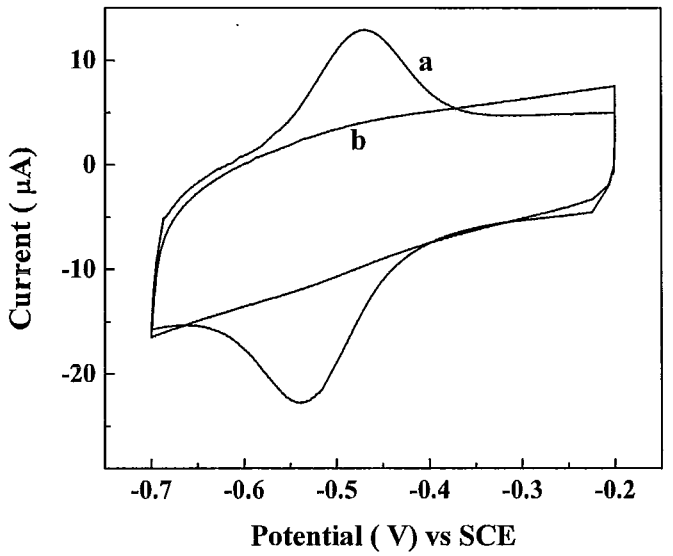

Figure 5-33 Cyclic voltammograms of film prepared from the 0.5 gL^{-1} chitosan solutions containing 2 gL^{-1} zinc oxide at a deposition voltage of 20 V with the deposition time of 10 seconds with (a) and without (b) immobilized glucose oxidase on the graphite electrode surface (diameter= 6mm) in phosphate buffered saline solution (PBS at pH 7.4 at a scan rate of 100 mV s^{-1}

Figure 5-33 shows cyclic voltammograms of film prepared from the 0.5 gL^{-1} chitosan solutions containing 2 gL^{-1} zinc oxide at a deposition voltage of 20 V with the deposition time of 10 seconds with (a) and without (b) immobilized glucose oxidase on the graphite electrode surface (diameter=6mm) in phosphate buffered saline solution (PBS) at pH 7.4 at a scan rate of 100 mV s^{-1}. Compared with modified ZnO/Chitosan electrode, the modified ZnO/Chitosan/GOx electrode exhibits a distinct response. A well defined pair of redox peaks was observed for the electrode, containing immobilized

enzyme. The latter are characteristic of the $FAD/FADH_2$ redox couple. The standard potential of the FAD/FAD_2 redox couple immobilized on the ZnO/Chitosan surface of E_0 =-0.48 V is very close to that expected in Rahman`s work [140].

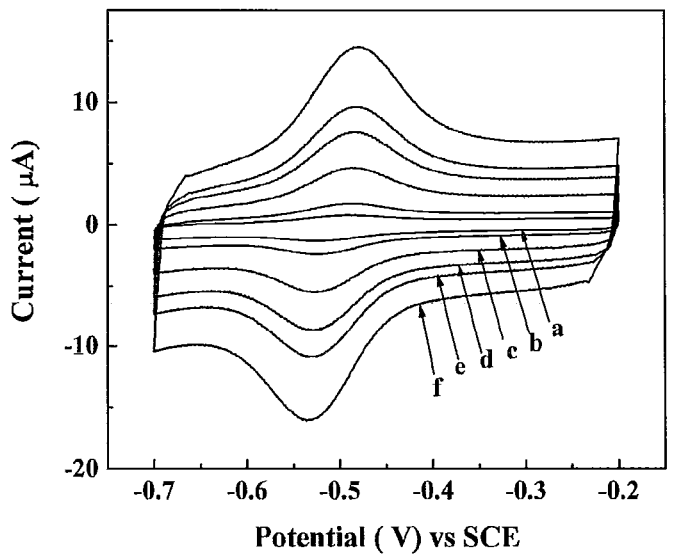

Figure 5-34 Cyclic voltammograms at the scan rates of 10 (a), 20 (b), 50 (c), 100 (d), 150 (e), 180 (f) mV s^{-1} for film prepared from the 0.5 gL^{-1} chitosan solution containing 1 gL^{-1} zinc oxide at a deposition voltage of 20 V with the deposition time of 10 seconds on the graphite electrode surface. GOx was immobilized from 50 g L^{-1} glucose oxidase solution in phosphate buffered saline solution (PBS). at pH 7.4

Figure 5-34 shows cyclic voltammograms of film prepared from the 0.5 g L^{-1} chitosan solutions containing 1 gL^{-1} zinc oxide at a deposition voltage of 20 V with the deposition time of 10 seconds and immobilized glucose oxidase on the graphite electrode

surface (diameter= 6mm) in phosphate buffered saline solution (PBS) at pH 7.4 at the scan rates of 10 (a), 20 (b), 50 (c), 100 (d), 150 (e), 180 (f) mV s^{-1}. With increasing scan rate, the cathodic peak and the anodic peak of GOx were nearly not shifted. Both the cathodic and anodic peaks currents were linearly proportional to the square root of the scan rate in the range from 10 mV/s to 180 mV/s.

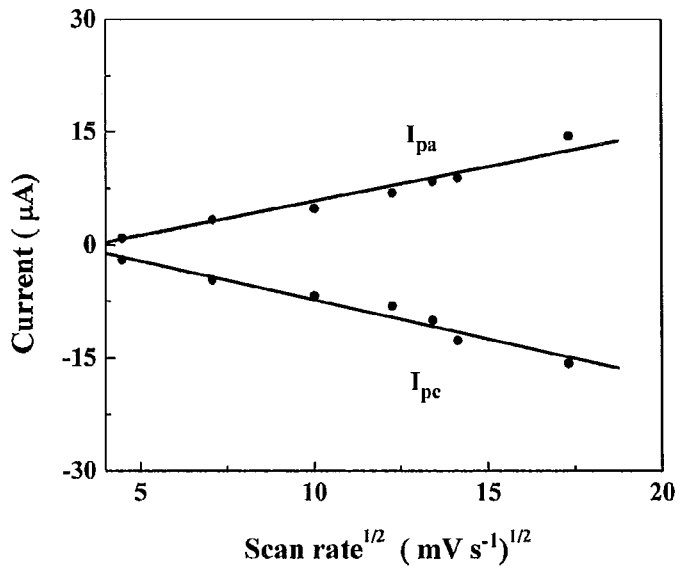

Figure 5-35 Plots of peak currents (anodic and cathodic) vs square root of scan rate for film prepared from the 0.5 gL^{-1} chitosan solutions containing 1 gL^{-1} zinc oxide at a deposition voltage of 20 V with the deposition time of 10 seconds on the graphite electrode. GOx was immobilized from 50g L^{-1} GOx solution in phosphate buffered saline solution (PBS), at pH 7.4.The data was obtained at the scan rates of 10, 20, 50, 80, 100, 150, 180, 300mV s^{-1}

Figure 5-35 shows plots of peak currents vs square root of scan rate for film prepared from the 0.5 gL^{-1} chitosan solutions containing 1 gL^{-1} zinc oxide at a deposition voltage of 20 V with the deposition time of 10 seconds and immobilized glucose oxidase on the graphite electrode surface (diameter= 6mm) in phosphate buffered saline solution (PBS) at pH 7.4 at the scan rates of 10, 20, 50, 80, 100, 150, 180, 300mV s^{-1}. The linear increase of redox current with respect to $(\text{scan rate})^{1/2}$ was observed and indicated diffusion-controlled process in agreement with Randel- Sevcik equation:

$$Ip = (2.69 * 10^5)\, n^{3/2} A\, D^{1/2} C\, v^{1/2} \qquad (5\text{-}11)$$

where Ip is peak current (Ipa anodic or Ipc cathodic), n is electron stoichiometry, A is electrode area , D is diffusion coefficient, C is surface concentration of GOx, and v is scan rate.

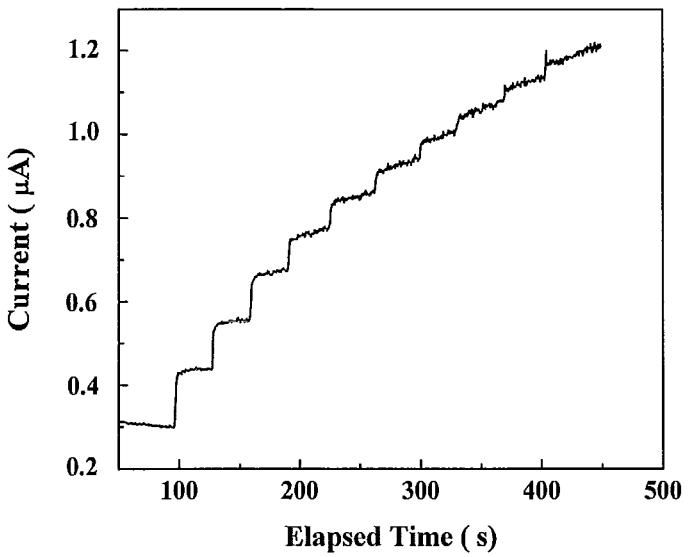

Figure 5-36 Amperometric response of film prepared from the 0.5 gL^{-1} chitosan solutions containing 1 gL^{-1} zinc oxide at a deposition voltage of 20 V with the deposition time of 10 seconds, containing immobilized glucose oxidase on the graphite electrode surface (diameter= 6mm) to successive additions of 1 mM glucose in phosphate buffered saline solution (PBS) at PH 7.4

Figure 5-36 shows amperometric response of film prepared from the 0.5 gL^{-1} chitosan solutions containing 1 gL^{-1} zinc oxide at a deposition voltage of 20 V with the deposition time of 10 seconds and immobilized glucose oxidase on the graphite electrode surface (diameter= 6mm) to successive additions of 1 mM glucose in phosphate buffered saline solution (PBS) at pH 7.4). It is demonstrated that the ZnO/Chitosan/GOx modified electrode exhibited relatively high sensitivity and stability. The electrocatalytic response towards glucose was attributed to the immobilized GOx on the substrate. The current

response was proportional to the concentration of glucose in the range of 0~5mM glucose PBS solution. In conclusion, ZnO/Chitosan based biocomposite electrode has been used for the immobilization of GOx for the fabrication of electrochemical glucose biosensor. It is suggested that ZnO/Chitosan films can be utilized for the immobilization of different enzymes and proteins with isoelectric point below pH=7 and fabrication of other biosensors and biomedical devices.

6 Conclusions

The main conclusions are summarized as follows:

- New electrochemical deposition methods have been developed for the fabrication and testing of electrochemical biosensors.
    - EPD has been utilized for the fabrication of chitosan/ alginic acid/ hyaluronic acid- GOx composite films. The mechanism of cathodic deposition of chitosan-GOx was based on electrophoresis of cationic chitosan in acidic solutions and film formation in the high pH region at the cathode surface. The mechanism of anodic deposition of alginic acid-GOx and hyaluronic acid- GOx was based on electrophoresis of anionic alginic acid and hyaluronic acid in basic solutions and film formation in the low pH region at the anode surface.
    - EPD has been utilized for the fabrication of chitosan - hemoglobin composite films. The mechanism of cathodic deposition of chitosan-hemoglobin was based on electrophoresis of cationic chitosan in acidic solutions and film formation in the high pH region at the cathode surface. SEM, FTIR, and CD spectra demonstrated that hemoglobin was immobilized on the chitosan matrix.

- EPD and ELD have been utilized for the fabrication of chitosan-zinc oxide nanocomposites for immobilization of enzymes. The deposition yield measurements, TGA, DTA, XRD, FTIR and SEM studies showed the formation of chitosan-zinc oxide nanocomposites. The deposit composition can be varied by the variation of the concentration of zinc oxide and zinc acetate in the suspensions. The method offers the advantages of room temperature processing for the fabrication of nanocomposites for biosensors applications. It was shown that nanocomposites, prepared by new electrochemical methods and containing zinc oxide can be used for electrostatic immobilization of enzymes.

- The feasibility of electrochemical immobilization of enzymes with polymers by EPD has been demonstrated. Electrochemical tests showed that the modified ZnO/Chitosan/GOx electrodes exhibited relatively high sensitivity and stability and can be utilized for applications of biosensors.

7 References:

1. M. Mehrvar, M. Abdi, *Recent development, Characteristics and potential applications of electrochemical biosensors.* Analytical Sciences, 2004. **20**: p. 1113-1126.
2. N. Ronkainen, H. Halsall, W. Heneman, *Electrochemical biosensors.* The Royal Society of Chemistry, 2010. **39**: p. 1747-1763.
3. P. Bartlett, J. Wiley & Sons, W. Sussex, Bioelectrochemistry Fundamentals, Experimental Techniques and Applications, 2008.
4. Saraju P. Mohanty, Elias Kougianos, *Biosensors: A Tutorial Review.*
5. A. Merce, L. Marques Carrera, L. Santors Romanholi, M. Lobo Recio, *Aqueous and solid complexes of iron (III) with hyaluronic acid:Potentiometric titrations and infrared spectroscopy studies.* Journal of Inorganic Biochemistry, 2002. **89**: p. 212-218.
6. Wang, Joseph, *Electrochemical biosensor: Towards point-of-care cancer diagnositics*, in *Biosensors and Bioelectronics* 2006. p. 1887-1892.
7. P. Bartlett, A review of the immobilization of enzymes in electropolymerized films, Jounal of Electroanalytical Chemistry, 362 (1993) 1-12.
8. Ronkainen, N. J., Halsall, H. B., and Heineman, W. R., *Electrochemical biosensors.* Chemical Society Reviews, 2010. **39**(5): p. 1747-1763.
9. Katharin R. Greenough, Andrew W. Skillen, Calum J. McNeil, *Potential glucose sensor for perioperative blood glucose control in diabetes mellitus.* Biosens & Bioelectron, 1994. **9**: p. 23-28.
10. Md. Mahbubur Rahman , A. J. Saleh Ahammad, Joon-Hyung Jin , Sang Jung Ahn , Jae-Joon Lee *A Comprehensive Review of Glucose Biosensors Based on Nanostructured Metal-Oxides.* Sensors, 2010. **10**: p. 4855-4886.
11. J. Wang, D.F. Thomas, A.Chen, *Nonenzymatic Electrochemical Glucose Sensor Based on Nanoporous PtPb Networks.* Anal. Chem, 2008. **80**: p. 997-1004.
12. G.S. Wilson, R. Gifford, *Biosensors for Real-Time in vivo Measurements.* Biosens. Bioelectron, 2005. **20**: p. 2388-2403.
13. Wang, Joseph., *Electrochemical glucose biosensors.* Chemical reviews, 2008. **108**: p. 814-825.
14. Audrey. Sassolas, Beatrice D. Leca-bouvier, Loic J. Blum, *DNA biosensors and microarrays.* Chemical reviews, 2008. **108**: p. 109-139.

15. M.Dijksma, W.P. van Bennekom, *Direct electrochemical immunosensors review.* Manuscript in preparation.
16. Francesco Ricci, Giulia Volpe, Laura Micheli, Giuseppe Palleschi, *A review on novel developments and applications of immunosensors in food analysis.* analytica chimica acta, 2007. **605**: p. 111-129.
17. Yongcheng, Liu, Tongyin, Yu, *Polymers and enzyme biosensors.* Polymer Reviews, 1997. **37**(3): p. 459-500.
18. H. Shinohara, T. Ohiba, M. Aizawa, *Sensors.* Sensors. Actuators, 1988. **13**(70).
19. D.T. Hoa, T.N. Suresh Kumar, N. S. Punekar, R.S. Srinivasa, R.Lal, A.Q. Contrctor, *Conducting polymer-based biosensors.* Analytical.Chemistry, 1992. **64**: p. 2645-2646.
20. S.E. Wolowacz, B.F.Y.Y. Hin, C.R. Lowe, *Electrochemical oxidation of cholesterol catalyzed by cholesterol oxidase with use of an artificial electron mediator.* Anal.Chem, 1993. **64**: p. 2367-2372.
21. Yano, H., *Effect of N-acetyl-glucosamine on wound healing in rats.* Mie medical journal, 1985. **35**: p. 53-56.
22. Peter, M. G., *Applications and environmental aspects of chitin and chitosan.* Journal of Macromolecular Science - Pure and Applied Chemistry, 1995. **A32**(4): p. 629.
23. Austin, P.R., *Solvents for and purification of chitin*, in *US Patent.* 1977, University of Delaware (Newark, DE) US.
24. Austin, P.R., *Chitin solvents and solubility parameters*, in *Chitin and chitosan and related enzymes*, J.P. Zikakis, Editor. 1984, Academic Press Inc.: Orlando. p. 227-237.
25. T. Sannan, K. Kurita, Y. Iwakura *Studies on chitin 1.* Makromolekulare Chemie Macromolecular Symposia, 1975. **176**: p. 1191-1195.
26. T. Sannan, K. Kurita, Y. Iwakura *Studies on chitin 2.* Makromolekulare Chemie Macromolecular Symposia, 1976. **177**: p. 3589-3600.
27. Madihally, Sundararajan V., and Matthew, Howard W. T., *Porous chitosan scaffolds for tissue engineering.* Biomaterials, 1999. **20**(12): p. 1133-1142.
28. Kyriacos, A. Athanasiou, Amita, R. Shah, Hernandez, R. Jason, and Richard, G. LeBaron, *BASIC SCIENCE OF ARTICULAR CARTILAGE REPAIR.* Clinics in sports medicine, 2001. **20**(2): p. 223-247.
29. M. Dornish, D. Kaplan, V. Skaugrud, *Standards and Guidelines for Biopolymers in Tissue-Engineered Medical Products.* Annals of the New York Academy of Sciences, 2001. **944**(Bioartificail Organs III: Tissue Sourcing, Immunoisolation and clinical trials): p. 388-397.

30. Kurita, Keisuke, *Controlled functionalization of the polysaccharide chitin.* Progress in Polymer Science, 2001. **26**(9): p. 1921-1971.
31. Marguerite Rinaudo, *Chitin and Chitosan :Properties and Applications.* ChemInform, 2007. **38**(27).
32. F. G. Pearson, R. H. Marchessault, C. Y. Liang,, *Infrared spectra of crystalline polysaccharides. V. Chitin.* Journal of Polymer Science, 1960. **43**(141): p. 101-116.
33. Francis Suh, and Matthew, Howard W. T., *Application of chitosan-based polysaccharide biomaterials in cartilage tissue engineering: a review.* Biomaterials, 2000. **21**(24): p. 2589-2598.
34. X. Pang, , and I. Zhitomirsky, *Electrodeposition of composite hydroxyapatite-chitosan films.* Materials Chemistry and Physics, 2005. **94**(2-3): p. 245-251.
35. X. Pang, and I. Zhitomisky, *Electrophoretic deposition of composite hydroxyapatite-chitosan coatings.* Materials Characterization, 2007. **58**(4): p. 339-348.
36. X.Pang, and, I.Zhitomirsky,*Electrodeposition of nanocomposite organic-inorganic coatings for biomedical applications.* International Journal of Nanoscience 2005. **4**(3): p. 409-418.
37. K.I. Draget, G. Skjåk-Bræk, B. E. Christensen, O. Gåserød , O. Smidsrød, *Swelling and partial solubilization of alginic acid gel beads in acidic buffer.* Carbohydrate Polymers, 1996. **29**(3): p. 209-215.
38. S.Thomas, *Alginates: a guide to the properties and uses of the different. alginate dressings available today.* Journal of Wound Care, 1992. **1**: p. 29-32.
39. M. Cheong, I. Zhitomirsky, *Electrodeposition of alginic acid and composite films.* Colloids and Surfaces A: Physicochemical and Engineering Aspects, 2008. **328**(1-3): p. 73-78.
40. K.Meyer, J.W. Palmer, *The polysaccharide of the vitreous humor.* The Journal of Biological Chemistry, 1934. **107**(3): p. 629-634.
41. B. Delpech, P. Bertrand, M.N. Courel, C. Chauzy, A. Delpech, *Hyaluronan: fundamental principles and applications in cance.* Journal of Internal Medicine, 1997. **242**(1): p. 41-48.
42. H. Kito, *Biocompatible coatings for luminal and outer surfaces of small-caliber artificial grafts.* Journal of Biomedical Materials Research, 1996. **30**(3): p. 321-330.
43. Schwarzacher, W., *Electrodeposition: A technology for the future.* The electrochemical Society Interface, 2006. **spring**.

44. O. Van der Biest, L.Vandeperre, *Electrophoretic deposition of materials.* Annual Review of Materials Science, 1999. **29**(1): p. 327-352.
45. A. Boccaccini, I.Zhitomirsky, *Application of electrophoretic and electrolytic deposition techniques in ceramics processing.* Current Opinion in Solid State and Materials Science, 2002. **6**(3): p. 251-260.
46. G. Payne, *Biopolymer-based materials: the nanoscale components and their hierarchical assembly.* Current Opinion in Chemical Biology, 2007. **11**(2): p. 214-219.
47. I.Zhitomirsky, *Cathodic electrodeposition of ceramic and organoceramic materials.Fundamental aspects.* Advances in Colloid and Interface Science, 2002. **97**(1-3): p. 277-315.
48. B.derjaguin, L. Landau, *Theory of the stability of strongly charged lyophobic sols and of the adhesion of strongly charged particles.* Acta Physicochimica, 1941. **14**: p. 633-662.
49. E. Verwey, J. Overbeek, *Theory of the stability of lyophobic colloids.* Amsterdam:Elsevier, 1948.
50. I. Zhitomirsky, L. Gal-Or, *Intermetallic and Ceramic Coatings.* Marcel Dekker Inc., New York, , 1999. **Chapter 3**.
51. I. Zhitomirsky, *Cathodic electrodeposition of ceramic and organoceramic materials. Fundamental aspects.* Advances in Colloid and Interface Science, 2002. **97**(1-3): p. 277-315.
52. H. Hamaker, *Formation of a deposit by electrophoresis.* Transactions of the Faraday Society 1940. **35**: p. 279-287.
53. H. Hamaker, and Verwey, E. J. W., *The Role of the Forces between the Particles in Electrodeposition and Other Phenomena.* Transactions of the Faraday Society 1940. **36**: p. 180-185.
54. K. Grandfield, I. Zhitomirsky, Materials Characterization, 2008. **59**(61).
55. C. Sanchez, G. De, A. Soler-Illia, F. Ribot, T. Lalot, CR. Mayer, V. Cabuil, *Designed hybrid organic-inorganic nanocomposites from functional nanobuilding blocks.* Chemistry of Materials, 2001. **13**(10): p. 3061-3083.
56. L. Beecroft, C. Ober, Chemistry of Materials, 1997(9): p. 1302.
57. R. Gangopadihyay, A. De, *Conducting polymer nanocomposites: A brief overview.* Chemistry of Materials, 2000. **12**(3): p. 608-622.
58. T. Sasaki, Y. Ebina, T. Tanada, M. Harada, M. Watanabe, *Layer-by-layer assembly of titania nanosheet/polycation composite films.* Chemistry of Materials, 2001. **13**(12): p. 4661-4667.

59. T. Cassagneau, F. Guerin, J. Fendler, *Prepareation and characterization of ultrathin films layer-by-layer self-assembled from graphite oxide nanoplatelets and polymers.* Langmuir, 2000. **16**(18): p. 7318-7324.
60. A. Dutta, T. Ho, L. Zhang, P. Stroeve, *Nucleation and growth of lead sulfide nano- and microcrystalites in supramolecular polymer assemblies.* Chemistry of Materials, 2000. **12**(4): p. 1042-1048.
61. T. Wang, M. Rubner, R. Cohen, *Polyelectrolyte multilayer nanoreactors for preparing silver nanoparticle composites : controlling metal concentration and nanoparticle size.* Langmuir, 2002. **18**(8): p. 3370-3375.
62. Zhitomirsky, I., *Electrophoretic deposition of organic-inorganic nanocomposites.* Journal of Materials Science, 2006. **41**: p. 8186-8195.
63. Zhitomirsky, I., *JOM-e* 52, 2000.
64. I. Zhitomirsky, A. Petric, *Cathodic electrolytic deposition of zirconia films.* Marterials Letter, 2000. **46**(1): p. 50.
65. I. Zhitomirsky, A. Petric, *Electrochemical processing and characterization of nickel hydroxide–polyelectrolyte films* Ceramics International, 2001. **27**: p. 149.
66. X. Pang, I. Zhitomirsky, *Electrodeposition of yttria/cobalt oxide and yttria/gold coatings onto ferritic stainless steel for SOFC interconnects* Surface and Coatings Technology, 2005. **195**: p. 138-140.
67. L.Wu, H. Yi, S. Li, G. Rubloff, W. Bentley, R. Ghodssi, G. F. Payne, *Spatially selective deposition of a reactive polysaccharide layer onto a patterned template.* Langmuir, 2003. **19**(3): p. 519.
68. R. Fernandes, L. Wu, T. Chen, H. Yi, G.W. Rubloff, R. Ghodssi, W.E. Bentley, G. F. Payne, *Electrochemically induced deposition of a polysaccharide hydrogel onto a patterned surface.* Langmuir, 2003. **19**(10): p. 4058-4062.
69. H. Yi, L. Wu, R. Ghodssi, G. Rubloff, G. Payne, W. Bentley, *A robust technique for assembly of nucleic acid hybridization chips based on electrochemically templated chitosan.* Analytical Chemistry, 2004. **76**(2): p. 365.
70. L.Wu, K. Lee, D. English, W. Losert, G. Payne, *Chitosan-mediated and spatially selective electrodeposition of nanoscale particles.* Langmuir, 2005. **21**(8): p. 3641-6.
71. H. Yi, L. Wu, E. Bentley, R. Ghodssi, G.W. Rubloff, J.N. Culver, G.F. Payne, *Biofabrication with chitosan.* Biomacromolecules, 2005. **6**(6).
72. A. Montembault, C. Viton, A. Domard, *Rheometric study of the gelation of chitosan in aqueous solution without cross-linking agent.* Biomacromolecules, 2005. **6**(2): p. 653-62.

73. R. Shacham. D. Avnir, D. Mandler, *Electrodeposition of methylated sol-gel films on conducting surfaces.* Advanced Materials, 1999. **11**(5): p. 384-388.
74. R. Fernandes, L.Q. Wu, T.H. Chen, H.M. Yi, G.W. Rubloff, R. Ghodssi, W.E. Bentley, G.F. Payne, *Electrochemically induced deposition of a polysaccharide hydrogel onto a patterned surface.* Langmuir, 2003. **19**(10): p. 4085-4062.
75. M. Chiong, I. Zhitomirsky, *Electrodeposition of alginic acid and composite films.* Colloids and Surfaces A:Physicochemical and Engineering Aspects, 2008. **328**: p. 73-78.
76. A. Osaka, T. Yoshioka, T. Yabuta, K. Tsuru, S. Hayakawa, *Blood compatibility of organic-inorganic biomedical materials.* Biomaterials, 2003. **24**: p. 2889.
77. P.M. Biesheuvel, H. Verweij, Journal of the American Ceramic Society, 1999. **82**: p. 1451.
78. X. Pang, T. Casagrande, I. Zhitomirsky, *Electrophoretic deposition of hydroxyapatite-CaSiO3-chitosan composite coatings.* Journal of Colloid and Interface Science, 2009. **330**: p. 323-329.
79. B. Alberts et, *Molecular Biology of the Cell.* Garland Science, New york, ed. 3rd Edition 1994.
80. L.Lulin, Journal of Internal Medicine, 1997. **242**(61).
81. G.D. Prestwich, K.P. Vercruysse, Pharmaceutical Science &Technology Today, 1998. **1**(42).
82. Y. Luo, K.R. Kirker, G.D. Prestwich, Journal of Controlled Release, 2000. **69**(169).
83. Myer, S.L., Annals of the Rheumatic Deseases 1995. **54**(433).
84. I. Zhitomirsky, Materials Letters, 2000. **42**(262).
85. Hamaker, H.C., *Trans. Faraday Soc.* 1940. **36**: p. 279.
86. I. Zhitomirsky,*Cathodic electrodeposition of ceramic and organoceramic materials. Fundamental aspects.* Advances in Colloid and Interface Science, 2002. **97**: p. 279-317.
87. X. Chu, A. Nikolov, D. Wasan, Journal of Chemical Physics, 1995. **103**: p. 6653.
88. I. Zhitomirsky, *Cathodic electrodeposition of organic-inorganic nanocomposites.* Journal of Materials Science, 2006. **41**: p. 8186-8195.
89. I. Zhitomirsky, *Cathodic electrodeposition of ceramic and organoceramic materials, Fundamental Aspects.* Advances in Colloid and Interface Science, 2002. **97**: p. 277-315.
90. H. Yi, L. Wu, W. Bentley, R. Ghodssi, G. Rubloff,J. Culver, G. Payne, *Biofabrication with chitosan.* Biomacromolecules, 2005. **6**: p. 2281-2894.

91. L. Fernandes,T. Wu, H. Chen, G. Rubloff, R. Ghodssi, W. Bentley, G. Payne, *Electrochemically induced deposition of a polysaccharide hydrogel onto a patterned surface.* Laugmuir, 2003. **19**: p. 4058-4062.
92. M. Cheong, I. Zhitomirsky, *Electrodeposition of alginic acid and composite films.* Colloids and Sufaces A: Physicochemical and Engineering Aspects 2008. **328**: p. 73-78.
93. I. Gorelikov, E. Kumacheva, *Electrodeposition of polymer-semiconductor nanocomposite films.* Chemistry of Materials, 2004. **16**: p. 4122-4127.
94. J. Park, X. Luo, H. Yi, T. Valentine, G. Payne, W. Bentley, R. Ghodssi, G. Rubloff, *Chitosan-mediated in situ biomolecule assembly in completely packaged microfluidic devices.* Lab on a Chip, 2006. **6**: p. 1315-1321.
95. Switzer, J., *Electrochemical synthesis of ceramic films and powders.* American Ceramic Society Bulletin, 1987. **66**: p. 1521-1524.
96. O. Van Der Biest, L. Vandeperre, *Electrophoretic deposition of materials.* Annual review of Materials Science, 1999. **29**: p. 327-352.
97. G. Therese, P. Kamath, *Electrochemical synthesis of metal oxides and hydroxides.* Chemistry of Materials Science, 2000. **29**: p. 327-352.
98. J. Wei, N. Nagarajan, I. Zhitomirsky, *Manganese oxide films for electrochemical supercapacitors.* Journal of Materials Processing Technology, 2007. **186**: p. 356-361.
99. B. Gu, C. Xu, G. Zhu, S. Liu, L. Chen, X.S. Li, *Tyrosinase immobilization on ZnO nanorods for phenol detection.* Journal of Physical Chemistry B, 2009. **113**: p. 377-381.
100. R. Khan, A. Kaushik, A. Ansari, G.Sumana, B. Malhotra, *Zinc oxide nanoparticles-chitosan composite film for cholesterol biosensor.* Analytica Chimica Acta 2008. **616**: p. 207-213.
101. P. Solanki, A. Kaushik, A. Ansari, M. Pandey, B. Malhotra, *Zinc oxide-chitosan nanobiocomposite for urea sensor.* Applied Physics Letters, 2008. **93**: p. 163903.
102. S. Chatman, B. Ryan, K. Poduska, *Selective formation of Ohmic junctions and Schottky barriers with electrodeposited ZnO.* Applied Physics Letters, 2008. **92**: p. 012103.
103. S. Limmer, E. Kulp, J. Switzer, *Epitaxial electrodeposition of ZnO on Au(111) from alkaline solution: exploiting amphoterism in Zn(II).* Langmuir, 2006. **22**: p. 10535-10539.
104. S. Peulon, D. Lincot, *Mechanistic study of cathodic electrodeposition of zinc oxide and zinc hydroxychloride films from oxygenated aqueous zinc chloride solutions.* Journal of the Electrochemical Society, 1998. **145**: p. 864-874.

105. T. Yoshida, D. Komatsu, N. Shimokawa, H. Minoura, *Mechanism of cathodic electrodeposition of zinc oxide thin films from aqueous zinc nitrate baths.* Thin Solid Films, 2004. **451-452**: p. 166-169.
106. F. Tang, Y. Sakka, T. Uchikoshi, *Electrophoretic deposition of aqueous nanosized zinc oxide suspensions on a zinc electrode.* Materials Research Bulletin, 2003. **38**: p. 207-212.
107. J. Lee, I. Leu, Y. Chung, M. Hon, *Fabrication of ordered ZnO hierarchical structures controlled via surface charge in the electrophoretic deposition process.* Nanotechnology, 2006. **17**: p. 4445-4450.
108. F. Sun, K. Sask, J. Brash, I. Zhitomirsky, *Surface modifications of Nitinol for biomedical applications.* Colloids and Sufaces B: Biointerfaces, 2008. **67**: p. 132-139.
109. Y. Kwon, K. Kim, C. Lim, K. Shim, *Characterization of ZnO nanopowders synthesized by the polymerized complex method via an organochemical route.* Journal of Ceramic Processing Research, 2002. **3**: p. 146-149.
110. R. Wahab, S. Ansari, Y. Kim, M. Song, H. Shin, *The role of pH variation on the growth of zinc oxide nanostructures.* Applied Surface Science, 2009. **255**: p. 4891-4896.
111. A. Umar, M. Rahman, M. Vaseem, Y. Hahn, *Ultra-sensitive cholesterol biosensor based on low-temperature grown ZnO nanoparticles.* Electrochemistry Communications, 2009. **11**: p. 118-121.
112. R. Murugan, S. Ramakrishna, *Bioresorbable composite bone paste using polysaccharide based nano hydroxyapatite.* Biomaterials, 2004. **25**: p. 3829-3835.
113. T. Coelho, R. Laus, A. Mangrich, V. Favere, M. Laranjeira, *Effect of heparin coating on epichlorohydrin cross-linked chitosan microspheres on the adsorption of copper (II) ions.* Reactive and Functional Polymers, 2007. **67**: p. 468-475.
114. B. Guan, W. Ni, Z. Wu, Y. Lai, *Removal of Mn(II) and Zn(II) ions from flue gas desulfurization wastewater with water-soluble chitosan.* Separation and Purification Technology, 2009. **65**: p. 269-274.
115. X. Wang, Y. Du, H. Liu, *Preparation, characterization and antimicrobial activity of chitosan-Zn complex.* Carbohydrate Polymers, 2004. **56**: p. 21-26.
116. D. Ramirez, P. Bartlett, M. Abdelsalam, H. Gomez, D. Lincot, *Electrochemical synthesis of macroporous zinc oxide layers by emplying hydrogen peroxide as oxygen precursor.* Physic Status Solidi (A) Applications and Materials, 2008. **205**: p. 2365-2370.
117. D. Ramirez, T. Pauporte, H. Gomez, D. Lincor, *Electrochemical growth of ZnO nanowires inside nanoporous alumina templates. A comparison with metallic Zn*

nanowires growth. Physic Status Solidi (A) Applications and Materials, 2008. **205**: p. 2371-2375.

118. T. Yoshida, J. Zhang, D. Komatsu, S. Sawatani, H. Minoura, T. Pauporte, D. Lincot, T. Oekermann, D. Schlettwein, H. Tada, D. Wohrle, K. Funabiki, M. Matsui, H. Miura, H. Yanagi, *Electrodeposition of inorganic/organic hybrid thin films.* Advanced Functional Materials, 2009. **19**: p. 17-43.
119. L. Wu, G. Payne, *Biofabrication: using biological materials and biocatalysts to contruct nanostructured assemblies.* Trends in Biotechnology, 2004. **22**: p. 593-599.
120. X. Pang, I. Zhitomirsky, M. Niewczas, *Cathodic electrolytic deposition of Zirconia films.* Surface and Coatings Technology, 2005. **195**: p. 138-146.
121. I. Zhitomirsky, M. Niewczas, A. Petric, *Electrodeposition of hybrid organic-inorganic films containing iron oxide.* Materials Letters, 2003. **57**: p. 1045-1050.
122. D. Shichukin, I. Radtchenko, G. Sukhorukov, *Synthesis of nanosized magnetic ferrite particles inside hollow polyelectrolyte capsules.* The Journal of Physical Chemistry B, 2002. **107**: p. 86-90.
123. K. Trimukhe, A. Varma, *Metal complexes of crosslinked chitosan:correlations between metal ion complexation values and thermal properties.* Carbohydrate Polymers, 2009. **75**: p. 63-70.
124. M. Cheong, I. Zhitomirsky, Electrodepostion of alginic acid and composite filmss, Colloids and Surfaces A :Physicochemical and Engineering Aspects **328** (2008) 73-78
125. I. Zhitomirsky, *Electrophoretic hydroxyapatite coatings and fibers.* Materials Letters, 2000. **42**: p. 262-271.
126. M. Gouda, S. Singh, A. Rao, M. Thakur, N. Karanth, *Thermal inactivation of glucose oxidase.* The Journal of Biological Chemistry, 2003. **278**(27): p. 24324-24333.
127. M. Rohr, C. Kubicek, J. Kominek, *Verlag Chemie Weinheim Muenchen.* Biotechnology, 1983. **3**: p. 455-456.
128. A. Turner, I. Karube, G. Wilson, Biosensor Fundamentals and Applications, 1987: p. 770.
129. M. Gouda, M. Thakur, N. Karanth, Biotechnology Letters, 1997. **11**: p. 653-655.
130. P. Yadav, R. Ajore, L. Bharadwaj, *Cross-linker mediated biofunctionalization of single wall carbon nanotubes with glucose oxidase.* Journal of Nanotechnology Online, 2009. **5**.

131. H. Yoon, S. Ko, J. Jang, *Field-effect-transistor sensor based on enzyme-functionalized polypyrrole nanotubes for glucose detection.* Journal of Physical Chemistry B, 2008. **112**: p. 9992-9997.
132. R. Murugan, S. Ramakrishna, *Bioresorbable composite bone paste using polysaccharide based nano hydroxyapatite.* Biomacromolecules, 2004. **25**: p. 3829-3835.
133. K. Wang, H. Yang, L. Zhu, Z. Ma, S. Xing, Q. Lv, J. Liao, C. Liu, W. Xing, *Direct electron transfer and electrocatalysis of glucose oxidase immobilized on glassy carbon electrode modified with Nafion and mesoporous carbon FDU-15.* Electrochinica Acta, 2009. **54**: p. 4626-4630.
134. T. Pathak, J. Kim, S. Lee, D. Baek, K. Paeng, *Preparation of alginic acid and metal alginate from algae and their comparative study.* Journal of Polymer and Environment, 2008. **16**: p. 198-204.
135. R. Ma, R. Epand, I. Zhitomirsky, *Electrodeposition of hyaluronic acid and hyaluronic acid-bovine serum albumin films from aqueous solutions.* Colloids and Sufaces B: Biointerfaces, 2008.
136. A.Maghraby, M. Ali, *Spectroscopic study of gamma irradiated bovine hemoglobin.* Radiation Physics and Chemistry, 2007. **76**: p. 1600-1605.
137. Marek, T., *Ftir-reflection absorption spectrometry of some proteins on a metallic copper surface.* Analytical Letters 2000. **33**: p. 1387-1398.
138. J. Li, L. Zhou, X. Han, J. Hu, H. Liu, J. Xu, *Direct electrochemistry of hemoglobin immobilized on siliceous mesostructured cellular foam.* Sensors and Actuators B, 2009. **138**: p. 545-549.
139. G. Artmann, L. Burns, J. Canaves, A. Temiz-Artmann, G. Schmid-Schonbein, S. Chien, C. Maggakis-Kelemen, *Circular dichroism spectra of human hemoglobin reveal a reversible structural transition at body temperature.* European Biophysics Journal, 2004. **33**: p. 490-496.
140. M. Rahman, A. Umar, K. Sawada, *Development of amperometric glucose biosensor based on glucose oxidase co-immobilized with multi-walled carbon nanotubes at low potential.* Sensors and Actuators B: Chemical, 2009. **137**: p. 327-333.